ioMosaic®
Minimizing risk. Maximizing potential.®

Analysis of PRV Stability In Relief Systems Part I

Detailed Dynamics

An ioMosaic® Publication

G. A. Melhem, Ph.D., FAIChE

This page is intentionally left empty

IOMOSAIC® CORPORATION

Analysis of PRV Stability In Relief Systems Part I
Detailed Dynamics

Process Safety and Risk Management Practices

authored by

G. A. Melhem, Ph.D., FAIChE

Printed December 27, 2024

This page is intentionally left empty

Notice:

This document was prepared by ioMosaic® Corporation (**ioMosaic**) for Public Release. This document represents ioMosaic's best judgment in light of information available and researched prior to the time of publication.

Opinions in this document are based in part upon data and information available in the open literature, data developed or measured by ioMosaic, and/or information obtained from ioMosaic's advisors and affiliates. The reader is advised that ioMosaic has not independently verified all the data or the information contained therein. This document must be read in its entirety. The reader understands that no assurances can be made that all liabilities have been identified. This document does not constitute a legal opinion.

No person has been authorized by ioMosaic to provide any information or make any representation not contained in this document. Any use the reader makes of this document, or any reliance upon or decisions to be made based upon this document are the responsibility of the reader. ioMosaic does not accept any responsibility for damages, if any, suffered by the reader based upon this document.

Revision Log:

Revision 1: January 3, 2022
Revision 2: September 25, 2024
Revision 3: October 18, 2024

...

Table of Contents

List of Figures

List of Tables

1 Introduction

Challenges associated with PRV stability issues for existing installations are not unique to any particular segment of the chemical process industry. This is an industry wide problem that has received a lot of attention from both OSHA and industry associations such as API, ACC, and AFPM. A consistent definition of what constitutes an Engineering Analysis is currently being proposed by API/ACC/AFPM for inclusion in the upcoming revision to API 520.

API, AFPM, and ACC are diligently working on the development of tools and recommended guidance on how to perform an Engineering Analysis to assess PRV stability for existing installations where the 3 % is exceeded. A consistent methodology is emerging that has a solid mathematical foundation and is installation specific.

2 PRV Stability, an Industry Wide Issue

We do not currently have sufficient evidence to confirm that existing PRV installations with excessive inlet pressure loss that is more than 3 % and less than the valve blowdown (where the reduced flow capacity is still sufficient) present an increased level of risk that is high enough to warrant physical changes to the installations. Physical changes to existing systems may actually increase the risk while modifications are being implemented and there is no assurance that such costly modifications will actually reduce the risk for all installations where the inlet pressure loss exceeds 3 %.

The issue of PRV stability is a complex one and has been the subject of active research in the last few decades. There is wide spread agreement among lead researchers that the 3 % rule is not sufficient to guarantee PRV stability. Numerous companies and organizations have been working diligently to develop and implement both screening and detailed modeling tools/methods to assess PRV stability. The list includes ioMosaic®, Chiyoda [2, 3], Darby/API, DIERS/AIChE, and Pentair [4, 5, 6, 7, 8] to name a few.

3 Common Threads

While the individual modeling details may differ between the various organizations, common threads are emerging that are clearly signaling that a solution may already exist but is in need of disciplined validation. It is clear that PRV stability is a dynamics problem which requires an understanding and coupling of the dynamics of the following components:

A- Pressure Source or Vessel/Equipment

B- Inlet Line

C- PRV

D- Discharge Line

Although all four components are equally important, the interaction of pressure wave phenomena in the inlet line with the valve disk motion is critical. How these four components are coupled together is also very important.

The dynamics of the pressure source are well understood, even for multiphase, reacting flows. We have developed commercial computer codes in wide use where the vessel dynamics have been benchmarked and heavily validated against test data and incident data.

The dynamics of flow in relief lines have also been well understood and researched in the literature, including numerical schemes for the solution of shock tube problems and waterhammer problems. The waterhammer problem encountered in rapid or sudden valve closure for example is very similar to our PRV stability problem. One dimensional solutions with gradual flow area changes should be sufficient to provide us with enough information about pressure wave interaction with the PRV disk. The one dimensional solutions are also practical for two-phase flow. We have developed numerous codes for the solution of waterhammer problems and explosions/shocks in one dimensional geometries. These solutions are also well validated and benchmarked. Note that it is possible to use simplified methods to assess the total pressure drop attributed to pressure waves for simple piping geometries.

The dynamics of the PRV itself are currently thought to be well represented with a single degree of freedom (SDOF) representation. The SDOF representation of the valve is also well researched and developed in the compressor literature for example. To properly model the valve dynamics, information pertaining to the geometry of the valve (disk area, spring constants, mass of the moving parts, valve lift vs. pressure, damping, etc.) must be known or need to be approximated. Issues related to restitution and sticktion may also need to be considered. All published PRV models (ioMosaic®, Chiyoda, Darby/API, EPRI, NRC) are very similar in concept.

4 Force Balance

The cross section and main components of a typical safety valve are shown in Figures 1 and 2. These Figures were adapted from Singh and Shak [9].

The movement of the valve disc depends on a force balance between the upward fluid force, F_{Up} and the downward spring and back pressure forces, F_{Dn}. The downward force consists of a back pressure force, a spring force, and the weight of the disc and moving parts:

$$\begin{aligned} F_{Dn} &= P_B A_B + K_s\left(x_o + x\right) + P_{atm} A_{bel} + m_D g + K_{sb} x \qquad (1)\\ &= P_B\left(A_D - A_{bel}\right) + K_s\left(x_o + x\right) + P_{atm} A_{bel} + m_D g + K_{sb} x \\ &= P_B A_D + K_s\left(x_o + x\right) + \left(P_{atm} - P_B\right) A_{bel} + m_D g + K_{sb} x \\ A_B &= A_D - A_{bel} \qquad (2)\\ A_D &= \pi R_D^2 \simeq \pi R_4^2 \qquad (3) \end{aligned}$$

Figure 1: Typical components of a safety valve

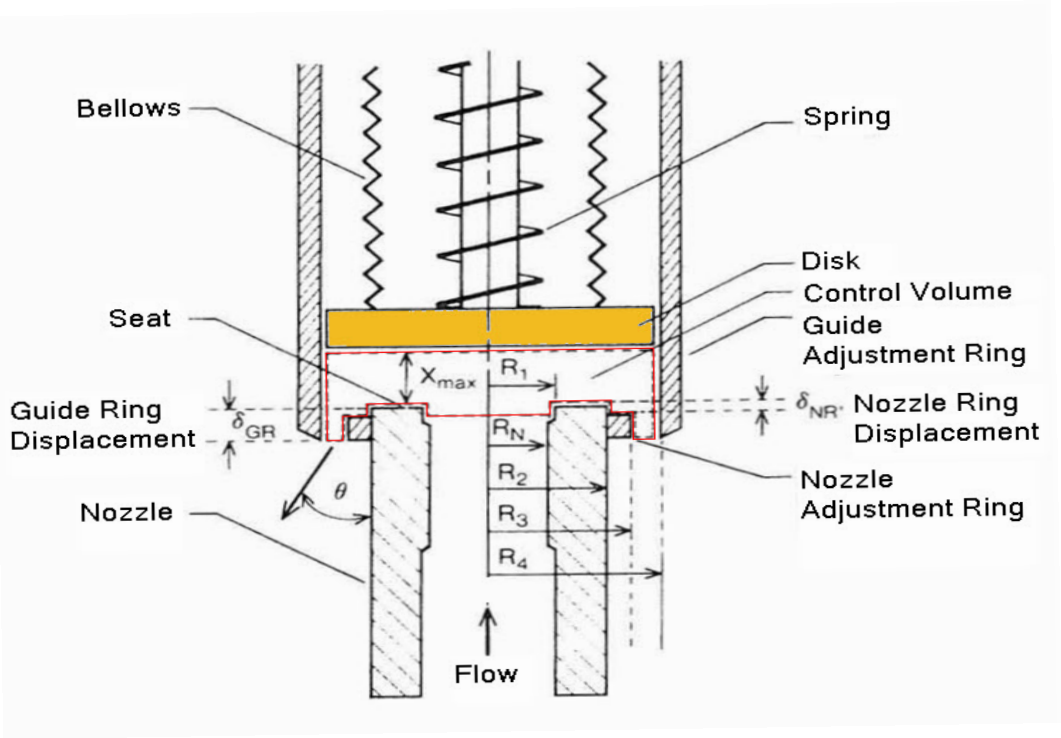

where, F_{Dn} is in N [1], A_B is the back pressure area in m^2, P_B is the back pressure acting on A_B in Pa, A_D is the entire disk back pressure area in m^2, R_D is the entire back pressure area radius in m, R_4 is the inner radius of the ring in m, K_s is the spring constant in $\mathrm{N/m}$, x_o is the initial compression of the valve spring at zero lift in m, x is valve stem displacement in m, P_{atm} is the atmospheric pressure in Pa, A_{bel} is the area of the disc enclosed by bellows in m^2, K_{sb} is the bellows stiffness constant in $\mathrm{N/m}$, $m_D$is the mass of the valve disc and moving parts in kg, and g is the acceleration due to gravity equal to $9.80665\ \mathrm{m/s^2}$.

The bellows will isolate the back of the disc from back pressure existing in the body bowl and prevent leakage of process fluid to the atmosphere. Bellows can only withstand specific levels of back pressure and can be damaged due to excessive back pressure. If the bellows are subjected to excessive back pressure and are damaged, the valve will then behave as a conventional valve, i.e. the entire disc area will be subjected to P_B. Due to the manufacturing tolerances, the effective area of the bellows could vary by as much as 10 percent. Typically $\frac{A_D}{A_{bel}} \simeq 1.10$. The bellows spring force can

Figure 2: Forces acting on the valve disc and control volume

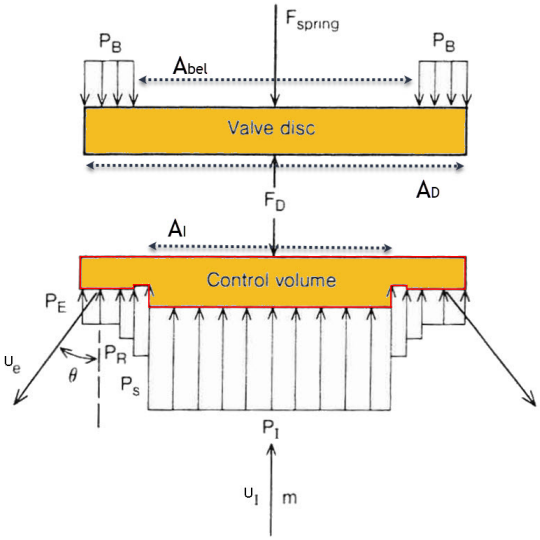

[1] 1 N = 1 kg $\frac{m}{s^2}$, 1 J = 1 N.m = 1 Pa.m^3 = 1 W.s

also be included in a similar manner to the helical spring force.

Bellows are typically designed for 1,000 cycles.
Bellows flexure can be caused by normal PRV cycling as well as turbulence inside the PRV body during normal venting and mechanical vibration from nearby equipment such as compressors and pumps. PRV chatter causing excessive high frequency PRV cycling of bellows can lead to bellows failure in a very short duration.

The upward fluid force F_{Up} acting on the disc depends on the fluid momentum and momentum transfer from the fluid stream impacting the disc. The momentum transfer to the disc is not easily represented using a one dimensional force balance and is strongly influenced by disk lift, disk geometry, and the blow down ring settings. The relative location of the rings [2] with respect to the seat level affects the fluid flow path and discharge angle as shown in Figure 1. F_{Up} can be calculated using the following expression:

$$F_{Up} = P_I A_I + P_S A_S + P_R A_R + P_E A_E + \dot{m}\, u_e \cos\theta + \frac{\dot{m}^2}{\rho_I A_I} \underbrace{-\rho_I A_I \left[(L_{\text{noz}} + x) \frac{du_I}{dt} + u_I \frac{dx}{dt} \right]}_{\text{typically negligible [10]}} \tag{4}$$

$$A_I = \pi R_1^2 \tag{5}$$

$$A_S = \pi R_2^2 - \pi R_1^2 \tag{6}$$

$$A_R = \pi R_3^2 - \pi R_2^2 \tag{7}$$

$$A_E = 2\pi R_3 \left(x + \delta_{NR}\right) \tag{8}$$

$$A_N = \pi R_N^2 \tag{9}$$

$$\theta_1 = 90 + (\theta_o - 90) \sqrt{\frac{x}{x_{max}}} \tag{10}$$

$$\theta_2 = \theta_o \frac{x}{x_{max}} \tag{11}$$

$$\theta = \omega\theta_1 + (1-\omega)\theta_2 \text{ where } 0 \le \omega \le 1 \tag{12}$$

where F_{Up} is in N, P_I is pressure at the inner seat area in Pa, A_I is the flow area at the inner seat radius in m^2, u_I is the fluid velocity in the nozzle, L_{noz} is the length of the nozzle, R_1 is the inner seat radius in m, P_S is pressure at the top surface of the valve seat in Pa, A_S is the area at the top surface of the valve seat in m^2, R_2 is the outer seat radius in m, P_R is pressure at the top surface of the nozzle ring in Pa, A_R is the area at the top surface of the nozzle ring in m^2, R_3 is the outer radius of the nozzle ring in m, P_E is the pressure in the annular flow area between the guide and nozzle rings in Pa, A_E is the annular flow area between the guide and nozzle rings in m^2, δ_{NR} is

[2] The guide and nozzle adjustment rings are threaded and can be moved up or down. The outer periphery of these rings is divided into uniform vertical notches. Each of the rings can be fixed at a desired vertical location relative to the valve seat level with the help of a locking screw through the valve body. The position of the adjustment rings with respect to valve seat level is typically specific by number of notches. The total number of notches on each ring corresponds to one revolution of that ring.

the nozzle ring displacement from the valve seat level in m, $\dot{m}$ is the mass flow rate in $\mathrm{kg/s}$, u_e is fluid exit velocity (typically sonic) at the annular flow area between the rings in $\mathrm{m/s}$, θ is the fluid exit discharge angle with respect to the vertical in degrees, θ_o is the fluid exist discharge angle from the vertical at full open valve stem position in degrees, x_{max} is the maximum valve lift in m, and ρ_I is the fluid density at the inner seat in $\mathrm{kg/m^3}$.For a valve with a constant nozzle flow area, R_1 and R_N are equal, i.e. $A_I = A_N$. The disk velocity will be zero, $\frac{dx}{dt} = 0$, if the valve is closed, $x = 0$, or the valve is at maximum lift, $x = x_{max}$.

The angle of flow θ is related to the blowdown setting of the valve. Different values of θ_0 lead to different values of implied blowdown for a specific valve geometry. If the blowdown is known, a value of θ_0 can be established to yield the specific value of that blowdown for liquid, vapor, or two phase flow.

The net upward force on the valve disk can then be calculated as follows:

$$\begin{aligned} F_{NET} &= F_{Up} - F_{Dn} \\ &= P_I A_I + P_S A_S + P_R A_R + P_E A_E + \dot{m}\, u_e \cos\theta + \frac{\dot{m}^2}{\rho_I A_I} \\ &\quad -P_B A_D - K_s x_o - K_s x - K_{sb} x - (P_{atm} - P_B)\, A_{bel} - m_D g \end{aligned} \tag{13}$$

The pressure at which the valve starts to open, P_{set}, can be obtained from a force balance at initial opening:

$$K_s x_o + m_D g = (P_{set} - P_{atm})\, A_I \tag{14}$$

Substituting the left hand side of the above equation in Equation 13, leads to the following general expression for the net upward force on the valve disk:

$$\begin{aligned} F_{NET} &= F_{Up} - F_{Dn} \\ &= (P_I - P_{set} + P_{atm})\, A_I + P_S A_S + P_R A_R + P_E A_E + \dot{m}\, u_e \cos\theta + \frac{\dot{m}^2}{\rho_I A_I} \\ &\quad -P_B A_D - K_s x - K_{sb} x - (P_{atm} - P_B)\, A_{bel} \end{aligned} \tag{15}$$

Values for A_S, A_R, and A_E are typically not readily available. We can rewrite those contributions as a function of the disk area minus the nozzle area:

$$\begin{aligned} F_{NET} &= F_{Up} - F_{Dn} \\ &= (P_I - P_{set} + P_{atm})\, A_I + \eta P_* (A_D - A_I) + \dot{m}\, u_e \cos\theta + \frac{\dot{m}^2}{\rho_I A_I} \\ &\quad -P_B A_D - K_s x - K_{sb} x - (P_{atm} - P_B)\, A_{bel} \end{aligned} \tag{16}$$

where P_* is the pressure on the upstream side of the disk in Pa and η is a conversion efficiency factor that can be determined experimentally for specific classes of pressure relief valves. η is used

to calibrate the model and to account for specific valve/disk geometry, etc. The value of P_* will depend on whether the flow is choked or not. The value of u_e can also be substituted with mass flow rate, fluid density, and the curtain flow area:

$$\begin{aligned} F_{NET} &= F_{Up} - F_{Dn} \\ &= \underbrace{P_I A_I + \eta P_* \left(A_D - A_I\right) + \frac{\dot{m}^2}{\rho_I A_I}}_{F_{Up,1}} + \underbrace{\left[\frac{\dot{m}^2}{2\pi R_1 x C_d \rho_e}\right]}_{F_{Up,2}} \cos\theta \\ &\quad - \left[\underbrace{P_B A_D + K_s x + K_{sb} x + \left(P_{atm} - P_B\right) A_{bel} + \left(P_{set} - P_{atm}\right) A_I}_{F_{Dn}}\right] \\ &= F_{Up,1} + F_{Up,2}\cos\theta - F_{Dn} \end{aligned} \tag{17}$$

If the pressure relief valve is operating stably during steady state at a specific disk lift x, then $F_{NET} = 0$:

$$0 = F_{Up,1} + F_{Up,2}\cos\theta - F_{Dn} \text{ or} \tag{18}$$

$$\cos\theta = \frac{F_{Dn} - F_{Up,1}}{F_{Up,2}} \tag{19}$$

As the valve seat starts to lift, the curtain area will be smaller than the nozzle flow area and will become the flow limiting area. It is also highly likely that the curtain area will continue to limit the flow even if the curtain area is larger than the nozzle area. The pressure relief valve nozzle area is typically smooth and has a flow discharge coefficient of near one. The curtain flow area involves a rough and irregular geometry and will have a discharge coefficient much lower than one. This is one of the primary reasons for why discharge coefficients for liquid flow are lower than gas discharge coefficients for pressure relief valves as the downstream valve geometry is not exposed during choked gas flow at the nozzle at maximum lift while the entire valve geometry is exposed to liquid flow which is almost always not choked at the nozzle.

As the fluid flows through the opening between the disk and the disk seat an additional area gets exposed to the fluid which leads to an increase in F_{UP}. This term is included in Equation 17 as $\eta P_* \left(A_D - A_I\right)$.

As the seat continues to lift this area becomes larger. When the curtain flow area becomes larger than the nozzle flow area, the flow will be limited by the nozzle flow area. We can calculate the disk lift at which both flow areas will be equal. Assuming that the discharge coefficient is well represented by the equation $C_d = \psi C_{d,max}$ where ψ is a constant, typically equal to 0.9, and $C_{d,max}$ is the discharge coefficient when the flow is regulated by the nozzle:

$$x_c = \frac{A_N}{2\pi R 1 \psi} \tag{20}$$

If the pressure relief valve has a constant nozzle diameter, i.e. $R_1 = R_N$, then x_c is equal to 1/2 the nozzle radius:

$$x_c = \frac{A_N}{2\pi R_N \psi} = \frac{\pi R_N^2}{2\pi R_N \psi} = \frac{R_N}{2\psi} \tag{21}$$

The effective curtain area, having a discharge coefficient of $C_d = \psi C_{d,max}$, can be expressed as a function of disk lift and nozzle flow area:

$$A_c = 2xC_d\sqrt{\pi A_N} \text{ where } x \leq \frac{R_N}{2\psi} \leq x_c \tag{22}$$

Typically A_I can be assumed to be equal to A_N. In addition, the disk and the bellows areas can be expressed as a multiple of A_N:

$$A_D \simeq 1.3A_N \tag{23}$$
$$A_{bel} \simeq 0.9A_D \simeq 1.17A_N \tag{24}$$

In order to calculate the mass flow rate through a flow area that is changing, we need to also have a reasonable value of a discharge coefficient. Recent CFD work for PRV performance and stability has shown a parabolic dependence of discharge coefficient vs lift, x/x_{max}.

$$C_d = C_{d,max}\left[\frac{x}{x_{max}}\right]^{\psi} \tag{25}$$

where ψ ranges from 0 to 1.

A different expression was used by Singh and Shak for the calculation of the discharge coefficient:

$$C_d = \psi C_{d,max} \quad \text{for} \quad x \leq x_c \tag{26}$$
$$C_d = C_{d,max} - (C_{d,max} - \psi C_{d,max})\frac{x_{max} - x}{x_{max} - x_c} \quad \text{for} \quad x > x_c \tag{27}$$

where ψ is an empirical parameter to be determined experimentally for a specific class of pressure relief valves. Singh and Shak report a value of $\psi = 0.9$ from their modeling efforts. For all liquid flow the value of P_* can be approximated by P_I. For choked gas or multiphase flow, if the flow is choked at the curtain area, then P_* can also be approximated by P_I. If the flow is choked at the nozzle, P_* can be approximated as P_B. Note that P_B represents the static pressure in the valve body bowl. The flow distribution in the body bowl has been shown to be three dimensional where flow separation and condensation is possible.

5 Single Degree of Freedom (SDOF) PRV Model

Using a single degree of freedom analysis to describe the motion of the valve disc, we can write the following equations:

$$\frac{dx}{dt} = u_d \tag{28}$$

$$m_D \frac{du_d}{dt} + C u_d = F_{NET} \tag{29}$$

where C is the coefficient of viscous damping in $\mathrm{Ns/m}$, and u_d is the speed of valve stem movement in $\mathrm{m/s}$.

It is typical to relate the coefficient of viscous damping to the critical damping coefficient for a spring-mass system:

$$C = \zeta C_{cr} \tag{30}$$

$$C_{cr} = 2 m_D \omega_n = \frac{2K_s}{\omega_n} = 2\sqrt{K_s m_D} \tag{31}$$

$$\omega_n = \sqrt{\frac{K_s}{m_D}} \tag{32}$$

where ζ is the viscous damping coefficient, dimensionless, typically set at 0.2, and ω_n is the undamped circular natural frequency in $\mathrm{radians/s}$. Other variables typically used in the context of single degree of freedom analysis include:

$$\tau_n = \frac{2\pi}{\omega_n} = 2\pi\sqrt{\frac{m_D}{K_s}} \tag{33}$$

$$f_n = \frac{1}{\tau_n} = \frac{\omega_n}{2\pi} = \frac{1}{2\pi}\sqrt{\frac{K_s}{m_D}} \tag{34}$$

where τ_n is the undamped natural period in s, and f_n is the undamped natural frequency in Hz where one Hz equals 1 cycle/second.

Using the above equations, we can now write an overall description of how the valve disc will move:

$$\frac{dx}{dt} = u_d \tag{35}$$

$$\frac{du_d}{dt} = \frac{1}{m_D}\left[F_{NET} - \zeta C_{cr} u_d\right] \tag{36}$$

When the valve disk is on the seat or at the upper stop, a coefficient of restitution is used to reverse the spindle direction [11]:

$$\frac{dx'}{dt} = -\beta \frac{dx}{dt} \tag{37}$$

where β is the coefficient of restitution (typically set at 0.01) and $x^{'}$ represents x after contact with the valve seat or upper stops.

6 Impact of Inlet and Discharge Piping

PRV stability is heavily influenced by the inlet and discharge piping configuration. Excessive inlet pressure loss or backpressure can cause PRV chatter and/or flutter. As the PRV starts to open, the pressure upstream of the PRV starts to decrease due to sudden expansion. This gives rise to an expansion wave that will travel upstream. As the expansion wave reaches the pressure source (Vessel) upstream, it reflects and travels back towards the PRV as a compression wave. The largest upstream pressure fluctuations are expected to occur during fast opening or closing of the PRV. Note that during the opening of the PRV, a delay is typically observed in backpressure buildup because of the time needed to fill body-bowl and the discharge piping. The interaction of the pressure wave and valve opening/closing can cause instability.

6.1 One Dimensional Fluid Dynamics Equations

Many practical relief systems problems include complex inlet and discharge relief piping geometries with area changes, orientation changes, and multiple piping segments. Total pressure loss in relief piping is required in order to estimate the pressure at the inlet and discharge of a relief device for capacity and stability calculations.

The total pressure loss can be calculated for a simple pipe with constant flow area using the method outlined by Singh and Shak [9] or Izuchi [2] described later in this document.

For complex piping, at least a solution of the one dimensional fluid flow equations (outlined later in this document) is required in order to properly calculate the total pressure loss. The dynamic solution of the pipe flow equations needs to be integrated with the single degree of freedom model of the valve and the time dependent solutions of the vessel dynamics. The one dimensional fluid flow equations are most applicable to geometries with gradual flow area changes and not abrupt flow area changes.

The boundary conditions connecting the vessel to the inlet line, the inlet line to the pressure relief valve inlet flange, and the pressure relief valve outlet flange to the discharge line must be carefully established. The one dimensional fluid dynamics equations can be written for single and/or multiphase flow. These equations include mass, momentum, energy, PVT, phase change, and phase equilibrium. We derive these equations for single phase flow next and extend them later to multiphase flow.

Continuity:

$$\frac{\partial}{\partial t}\left[\rho A\right] + \frac{\partial}{\partial x}\left[\rho u A\right] = \frac{\dot{m}_{in} - \dot{m}_{out}}{\Delta x} \tag{38}$$

or

$$\frac{\partial \rho}{\partial t} = -\frac{\rho u}{A}\frac{\partial A}{\partial x} - u\frac{\partial \rho}{\partial x} - \rho\frac{\partial u}{\partial x} + \frac{\dot{m}_{in} - \dot{m}_{out}}{A\Delta x} \tag{39}$$

Under steady state assumptions:

$$\frac{d\dot{m}}{dx} = \frac{\dot{m}_{in} - \dot{m}_{out}}{\Delta x} \tag{40}$$

or

$$\dot{m} = \rho u A = \dot{m}_{in} - \dot{m}_{out} \tag{41}$$

Momentum:

$$\frac{\partial}{\partial t}\left[\rho u A\right] + \frac{\partial}{\partial x}\left[\rho u^2 A + PA\right] = P\frac{\partial A}{\partial x} - A\frac{dF}{dx} - \rho g A\sin\theta + \left(\frac{\dot{m}_{in}u_{in} - \dot{m}_{out}u_{out}}{\Delta x}\right) \tag{42}$$

Without mass flow in or out of the system, the momentum equation becomes:

$$\frac{\partial}{\partial t}\left[\rho u\right] + \frac{1}{A}\frac{\partial}{\partial x}\left[\rho u^2 A\right] = -\frac{\partial P}{\partial x} - \frac{dF}{dx} - \rho g\sin\theta \tag{43}$$

where $\frac{dF}{dx}$ is the sum of pressure losses per length of pipe due to friction, turbulence, and/or fittings:

$$\frac{dF}{dx} = \left(\frac{dP}{dx}\right)_{friction} + \left(\frac{dP}{dx}\right)_{fittings} = \frac{\rho u|u| f}{\sqrt{\left(\frac{A}{\pi}\right)}} + \frac{1}{2}\rho u|u|\frac{K}{L} \tag{44}$$

Note that $\sin\theta$ is used to express the change of elevation with axial distance, where θ is the flow angle with respect to the horizontal:

$$\sin\theta = \frac{dz}{dx} \tag{45}$$

Under steady state, the momentum equation is often written as follows:

$$\underbrace{\frac{dP}{dx}}_{\text{Pressure Loss}} = -\underbrace{\frac{1}{A}\frac{d}{dx}\left[\dot{m}u\right]}_{\text{acceleration}} - \underbrace{\frac{dF}{dx}}_{\text{friction and fittings}} - \underbrace{\rho g\sin\theta}_{\text{gravity}} \tag{46}$$

The momentum equation can be simplified to yield a direct expression for the change of flow velocity with respect to time by replacing the change of density with respect to time using the mass continuity equation:

$$\frac{\partial u}{\partial t} = -u\frac{\partial u}{\partial x} - \frac{1}{\rho}\frac{\partial P}{\partial x} - g\sin\theta - \frac{fu|u|}{\sqrt{A/\pi}} - \frac{1}{2}u|u|\frac{K}{L} \tag{47}$$

For steady flow, the above equation can be reduced further:

$$udu + \frac{dP}{\rho} + gdz + dF = \frac{1}{2}du^2 + \frac{dP}{\rho} + gdz + dF = 0 \tag{48}$$

This form of of the momentum equation is also known as Euler's equation or Bernoulli's equation (without friction). This form is independent of the energy equation (first law of thermodynamics). It is based on Newton's second law of motion. It applies to an incompressible fluid and does not consider systems in which there is heat or work interaction between the system and its surroundings.

Energy:

$$\frac{\partial}{\partial t}\left[\rho A\left(e + \frac{u^2}{2} + gz\right)\right] + \frac{\partial}{\partial x}\left[\rho uA\left(h + \frac{u^2}{2} + gz\right)\right] = \frac{d\Omega}{dx} + \frac{d\Xi}{dx} \tag{49}$$

where $d\Omega/dx$ is the net energy exchange due to heat transfer, chemical reaction(s), and shaft work. $d\Xi$ represents the net change in energy to the system caused by mass inflow and outflow. $d\Omega/dx$ is typically expressed as:

$$\frac{d\Omega}{dx} = \frac{dq}{dx} + \frac{dq_{rxn}}{dx} - \frac{dw}{dx} \tag{50}$$

$$= \underbrace{U\pi D\left(T_a - T\right)}_{\text{heat from surroundings}} + \underbrace{\frac{dq_{rxn}}{dx}}_{\text{chemical reactions}} - \underbrace{\frac{dw}{dx}}_{\text{shaft work lost}} \tag{51}$$

In SI units, $\frac{d\Omega}{dx}$ will have units of $\mathrm{W/m}$ or $\mathrm{kg.m/s^3}$. For combustion reactions, dq_{rxn} is typically expressed using a flame speed:

$$\frac{dq_{rxn}}{dx} = \Delta h_{rxn}\frac{S_f A\rho}{dx} \tag{52}$$

$d\Xi$ is expressed as:

$$\frac{d\Xi}{dx} = \frac{\dot{m}_{in}}{\Delta x}\left(h_{in} + \frac{u_{in}^2}{2} + gz_{in}\right) - \frac{\dot{m}_{out}}{\Delta x}\left(h_{out} + \frac{u_{out}^2}{2} + gz_{out}\right) \tag{53}$$

At steady state and without mass gain or loss by the system, $\rho u A$ is constant, and the energy equation is typically written as follows for steady pipe flow:

$$\frac{d}{dx}\left(\dot{m}h + \dot{m}\frac{u^2}{2}\right) = \frac{d\Omega}{dx} - \dot{m}g\sin\theta \tag{54}$$

The specific enthalpy h can be replaced with specific energy $h = e + \frac{P}{\rho}$:

$$de + \frac{dP}{\rho} + \frac{d}{2}u^2 + gdz = \frac{1}{\dot{m}}d\Omega \tag{55}$$

We note that the steady state energy balance contains the same expression derived from the momentum equation for Bernoulli's equation. If we subtract Bernoulli's equation from the energy equation, it becomes obvious that energy dissipated as friction and/or turbulence during flow can cause an increase in the fluid's internal energy or temperature when work and heat transfer are zero.

$$de = \underbrace{\frac{1}{\dot{m}}d\Omega}_{zero} + dF = dF \tag{56}$$

Energy dissipation due to irreversible losses of fluid flow is also associated with entropy. There are also entropy changes related to internal irreversibles processes associated with degradation of energy from non-equilibrium processes, etc.

$$ds = \underbrace{ds_{ext}}_{\text{positive or negative}} + \underbrace{ds_{int}}_{\text{positive or zero}} \tag{57}$$

The rate of entropy generation indicates the degree of the irreversibility of the process and can be related to enthalpy change:

$$dh = Tds + vdP = \underbrace{ds_{ext}}_{\text{external}} + \underbrace{ds_{int}}_{\text{internal}} + \frac{dP}{\rho} \tag{58}$$

Replacing dq with Tds_{ext} and using the above expression for dh as a function of entropy, we can show that energy dissipation by friction and/or turbulence will increase the internal energy of the fluid and its entropy:

$$de = Tds_{int} = dF \tag{59}$$

The energy equation can also be solved directly for internal energy by substituting $h = e + P/\rho$. For the case where heat exchange due to chemical reactions is zero the following expression is obtained:

$$\frac{\partial e}{\partial t} = -u\frac{\partial e}{\partial x} - \frac{P}{\rho A}\frac{\partial}{\partial x}(Au) + \frac{u^3 f}{\sqrt{A/\pi}} + \frac{1}{2}\frac{u^3 K}{L} + \frac{\pi DU(T_s - T)}{\rho A} - \frac{1}{\rho A}\frac{dw}{dx} \tag{60}$$

We can further express the above equation as a function of temperature or pressure. For an ideal gas with a constant heat capacity, the above equation can be solved directly for temperature:

$$\frac{\partial T}{\partial t} = -u\frac{\partial T}{\partial x} - \frac{P}{\rho A C_v}\frac{\partial}{\partial x}(Au) + \frac{u^3 f}{C_v\sqrt{A/\pi}} + \frac{1}{2C_v}\frac{u^3 K}{L} + \frac{\pi DU(T_s - T)}{\rho A C_v} - \frac{1}{\rho A C_v}\frac{dw}{dx} \tag{61}$$

The friction and/or turbulence heating terms are typically ignored in pipe flow calculations. However, its impact on temperature may be important for high speed gas flow and long pipelines, especially with high pipe surface roughness. Using pressure and density the energy equation can be written as follows for an ideal gas with constant heat capacity:

$$\frac{\partial P}{\partial t} = -u\frac{\partial P}{\partial x} + c^2\left[u\frac{\partial \rho}{\partial x} + \frac{\partial \rho}{\partial t}\right] + \rho(\gamma - 1)\left[\frac{u^3 f}{\sqrt{A/\pi}} + \frac{1}{2}\frac{u^3 K}{L} + \frac{\pi DU(T_s - T)}{\rho A} - \frac{1}{\rho A}\frac{dw}{dx}\right] \tag{62}$$

Note that the square of the speed of sound c is equal to $\gamma\frac{P}{\rho}$

Equation of State:

An equation of state is needed to relate pressure, temperature, and density. For illustration purposes, we will use a constant heat capacity ideal gas equation of state expressed in terms of specific energy and enthalpy.

$$\gamma = \frac{C_p}{C_v} = \frac{C_p}{C_p - R_g} \tag{63}$$

or

$$C_p = R_g\frac{\gamma}{\gamma - 1} \text{ or } c_p = \frac{R_g}{M_w}\frac{\gamma}{\gamma - 1} \tag{64}$$

The pressure, specific enthalpy, and specific internal energy can be calculated using the following expressions:

$$P = \rho e(\gamma - 1) = \frac{\rho R_g T}{M_w} \tag{65}$$

$$e = \frac{P}{\rho(\gamma - 1)} = \frac{R_g T}{M_w(\gamma - 1)} \tag{66}$$

$$h = e + \frac{P}{\rho} = \frac{P}{\rho}\left(\frac{\gamma}{\gamma - 1}\right) = \frac{R_g T}{M_w}\left(\frac{\gamma}{\gamma - 1}\right) \tag{67}$$

$$E = \rho\left[e + \frac{u^2}{2}\right] = \frac{\rho u^2}{2} + \rho e = \frac{\rho u^2}{2} + \frac{P}{\gamma - 1} \tag{68}$$

where E is energy per unit volume. It can be shown that the speed of sound in a constant flow area pipe under adiabatic conditions is equal to:

$$c^2 = \frac{\gamma R_g T}{M_w} = \left[\frac{\partial P}{\partial \rho}\right]_s = \frac{1}{\rho \kappa_s} = \gamma \frac{P}{\rho} \tag{69}$$

For an ideal gas undergoing an isentropic change in state (compression or expansion), the initial and final state densities are correlated as follows:

$$\frac{P}{\rho^\gamma} = \text{constant} = \frac{P_1}{\rho_1^\gamma} = \frac{P_2}{\rho_2^\gamma} \tag{70}$$

We can also relate than change in pressure with respect to axial distance to the speed of sound for isentropic flow:

$$c^2 = \left[\frac{\partial P}{\partial \rho}\right]_s = \frac{dP}{d\rho} \tag{71}$$

$$\frac{1}{\rho}\frac{\partial P}{\partial x} = \frac{1}{\rho}\frac{dP}{d\rho}\frac{\partial \rho}{\partial x} = \frac{c^2}{\rho}\frac{\partial \rho}{\partial x} \tag{72}$$

$$\frac{\partial P}{\partial x} = c^2 \frac{\partial \rho}{\partial x} \tag{73}$$

The same expression for $\partial P/\partial x$ can also be obtained by differentiating Equation 70 with respect to axial distance:

$$\frac{\partial}{\partial x}\left(\frac{P}{\rho^\gamma}\right) = \frac{1}{\rho^\gamma}\left[\frac{\partial P}{\partial x} - \underbrace{\frac{\gamma P}{\rho}}_{c^2}\frac{\partial \rho}{\partial x}\right] = 0 \tag{74}$$

This leads to the expression:

$$\frac{\partial P}{\partial x} = \frac{\gamma P}{\rho}\frac{\partial \rho}{\partial x} = c^2 \frac{\partial \rho}{\partial x} \tag{75}$$

For an ideal gas undergoing a constant stagnation enthalpy change, the change of temperature with respect axial distance can be related to the change in velocity with respect to axial distance:

$$\frac{\partial}{\partial x}\left(h + \frac{1}{2}u^2\right) = C_p \frac{\partial T}{\partial x} + u\frac{\partial u}{\partial x} = 0 \tag{76}$$

6.2 Non-ideal Fluid Pressure Explicit 1D Flow Equations

The 1D equations presented earlier for an ideal gas can be also written for a real fluid where compressibility effects are important. The equations need to allow for the calculation of compressibility as a function of temperature, pressure, and composition. As a result, we write these equations in terms of velocity, pressure, temperature, and calculate the density directly from an equation of state:

Momentum:

$$\frac{\partial u}{\partial t} = -u\frac{\partial u}{\partial x} - \frac{1}{\rho}\frac{\partial P}{\partial x} - \frac{2f|u|u}{D_h} - g\sin\theta - \frac{1}{2}\frac{|u|uK}{L} \tag{77}$$

Mass:

$$\frac{\partial P}{\partial t} = -u\frac{\partial P}{\partial x} - \rho c_e^2\frac{\partial u}{\partial x} - \frac{\rho c_e^2}{A}\left(\frac{\partial A}{\partial t} + u\frac{\partial A}{\partial x}\right) + \frac{\beta c_e^2}{c_p}F_1 \quad \text{or} \tag{78}$$

$$\frac{\partial \rho}{\partial t} = -u\frac{\partial \rho}{\partial x} - \rho\frac{\partial u}{\partial x} - \frac{\rho}{A}\left(\frac{\partial A}{\partial t} + u\frac{\partial A}{\partial x}\right) \tag{79}$$

Energy:

$$\frac{\partial T}{\partial t} = -u\frac{\partial T}{\partial x} - \frac{\beta T c_e^2}{c_p}\frac{\partial u}{\partial x} - \frac{\beta T c_e^2}{A c_p}\left(\frac{\partial A}{\partial t} + u\frac{\partial A}{\partial x}\right) + \frac{c_e^2\kappa_T}{c_p}F_1 \quad \text{or} \tag{80}$$

$$\frac{\partial h_0}{\partial t} = -u\frac{\partial h_0}{\partial x} + \frac{1}{\rho}\frac{\partial P}{\partial t} + \frac{k}{\rho}\left(\frac{\partial^2 T}{\partial x^2} + \frac{1}{A}\frac{\partial A}{\partial x}\frac{\partial T}{\partial x}\right) + \frac{\frac{dQ_{in}}{dt} - \frac{dQ_{out}}{dt}}{\rho A} - \frac{1}{\rho A}\frac{dW}{dx} \tag{81}$$

PVT:

$$\rho = f(T, P, x_i) \tag{82}$$

where:

$$h_0 = \frac{P}{\rho} + e + \frac{1}{2}u^2 + gz \tag{83}$$

$$\frac{c_e^2\kappa_T}{c_p} = \frac{1}{\rho c_v} \tag{84}$$

$$\frac{\beta T c_e^2}{c_p} = \frac{1}{c_v}\frac{\beta T}{\rho\kappa_T} \tag{85}$$

$$F_1 = k\left(\frac{\partial^2 T}{\partial x^2} + \frac{1}{A}\frac{\partial A}{\partial x}\frac{\partial T}{\partial x}\right) + \frac{2f\rho u^3}{D_h} + \frac{1}{2}\frac{\rho u^3 K}{L} + \frac{\pi D_h U\left(T_s - T\right)}{A} + \frac{\frac{dQ_{in}}{dt} - \frac{dQ_{out}}{dt}}{A} - \frac{1}{A}\frac{dW}{dx} \tag{86}$$

h_0 is the specific fluid enthalpy, e is the specific fluid internal energy, z is the elevation, A is the flow area, x is the axial distance, θ is the flow angle with respect to horizontal, f is the Fanning friction factor, D_h is the hydraulic flow diameter, L is the length of the pipe segment, ρ is the fluid mass density, P is the fluid static pressure, T is the fluid temperature, u is the flow velocity, c_p and c_v are the specific fluid heat capacities at constant pressure and constant volume, β is the volume expansion coefficient, κ_T is the fluid isothermal compressibility, K is the number of velocity head losses associated with fittings, k is the fluid thermal conductivity, U is the overall heat transfer coefficient from the pipe wall to the surroundings, T_s is the surroundings temperature, W is the work done by the fluid on the surroundings, dQ/dt is the heating rate, and c_e is the effective fluid/pipe speed of sound which accounts for pipe flexibility. F_1 includes the heating effect of conduction in the fluid, wall friction, and wall heating on the fluid density [12]. F_1 is an energy dissipation term (entropy production) and is usually negligible for liquids.

Equation 80 can be expressed in terms c_v instead of c_p:

$$\frac{\partial T}{\partial t} = -u\frac{\partial T}{\partial x} - \frac{1}{c_v}\frac{\beta T}{\rho\kappa_T}\frac{\partial u}{\partial x} - \frac{1}{c_v}\frac{\beta T}{\rho\kappa_T}\frac{1}{A}\left(\frac{\partial A}{\partial t} + u\frac{\partial A}{\partial x}\right) + \frac{1}{\rho c_v}F_1 \tag{87}$$

For an ideal gas, $\beta = 1/T$ and $\kappa_T = 1/P$:

$$\frac{\partial T}{\partial t} = -u\frac{\partial T}{\partial x} - \frac{P}{\rho c_v}\frac{\partial u}{\partial x} - \frac{P}{\rho c_v}\frac{1}{A}\left(\frac{\partial A}{\partial t} + u\frac{\partial A}{\partial x}\right) + \frac{1}{\rho c_v}F_1 \tag{88}$$

If we assume A does not change with time, we can further reduce the above equation for $\partial T/\partial t$:

$$\frac{\partial T}{\partial t} = -u\frac{\partial T}{\partial x} - \frac{P}{\rho c_v}\frac{1}{A}\frac{\partial\left[Au\right]}{\partial x} + \frac{1}{\rho c_v}F_1 \tag{89}$$

The change of flow area with time, $\frac{\partial A}{\partial t}$, is usually neglected. There are some unique scenarios where $\frac{\partial A}{\partial t}$ should be calculated such as in the case of high pressure subcooled flow systems in long pipelines. During flow and as the pipeline pressure drops to the saturation conditions, the slight contraction of the pipe flow area over time can result in a large volume change over the entire pipeline. This can lead to sustained flow for long periods of time. The change of flow area will depend on the pipe wall temperature and internal pipe pressure:

$$\frac{\partial A}{\partial t} = 2\alpha_s A\frac{\partial T}{\partial t} + \frac{D_i}{\delta}\frac{A}{E_s}\left[1.25 - \nu\right]\frac{\partial P}{\partial t} \tag{90}$$

where α_s is the pipeline wall linear thermal expansion coefficient, D_i is the internal pipe flow diameter, δ is the pipe wall thickness, E_s is the pipe modulus of elasticity, and ν is Poisson's ratio ($\simeq 0.3$).

7 Body Bowl Choking in Gas Systems

Body bowl choking can be an issue for both vapor and twophase flow. This is particularly important for twophase flow as the body bowl choking pressure becomes the back pressure impacting the

force balance on the PRV disk and can negatively impact PRV stability, especially for conventional spring loaded pressure relief valves [13].

Figure 3: Body bowl choking regions for an ideal gas

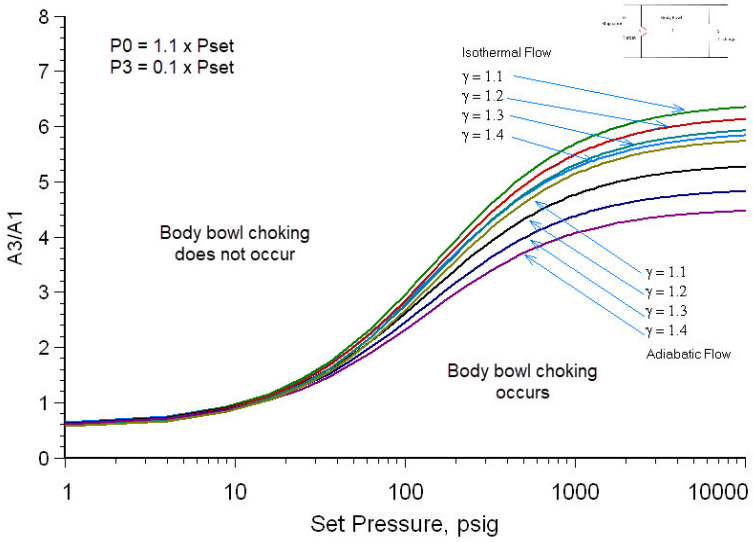

Source: ioMosaic® [14]

Choking pressure ratios are wider for twophase flow than for gas or vapor flow which is why pressure relief valves used in twophase flow service are almost always of the balanced type. Body bowl choking becomes more pronounced at higher pressure relief valve set pressures (see Figure 3).

Pressure relief valves with large nozzle flow areas relative to discharge flange connections [3] flow areas are more susceptible to body bowl choking. This includes pressure relief valves with J, L, P, Q, R, and T flow orifice areas designations [15]. To properly capture body bowl choking, a small section of pipe should be added to the 1D piping representation of the relief line [16, 14]. It is recognized that the flow patterns in the valve body can be complex [17] and that a 1D representation is only useful to capture a reasonable representative pressure value that can be used as the back pressure on the valve disc [18].

We illustrate some of the concepts of body bowl choking using all gas flow for simplicity. Figure 4 illustrates body bowl choking for a gas system with a ratio of outlet flange flow area to nozzle flow area of 2. Two choke points are identified: (a) a nozzle choke point and (b) a body bowl choke point.

In Figure 5 we add a discharge line that has the same diameter as the PRV outlet flange. Adding a discharge line with the same diameter as the PRV outlet flange shifts the choke point to the end of the line. Longer discharge

Figure 4: Body bowl choking for a gas system without a discharge line

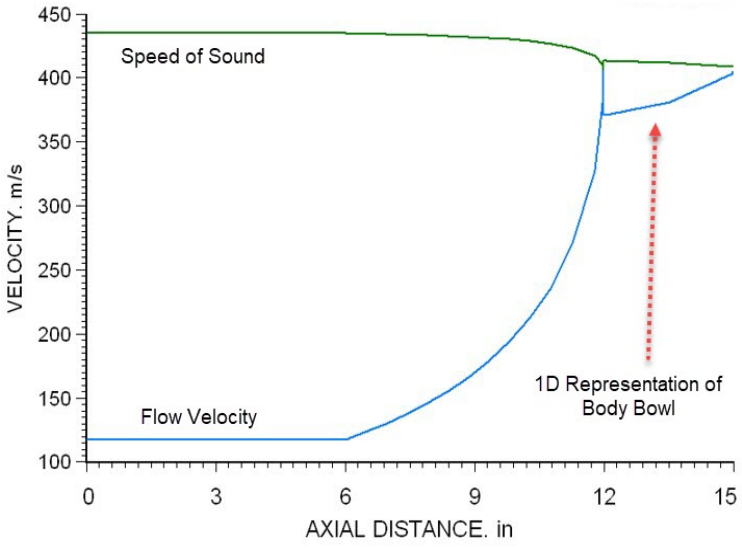

Source: Process Safety Office® SuperChems

[3] Often referred to as β ratios.

line segments can cause the choke point to shift to different locations/segments downstream of the first choke point that is regulating the flow. A very long discharge line segment can cause significant loss of pressure leading to subsonic flow in upstream locations and can ultimately become the flow regulating piping segment. This is common in relief lines where the relief device is only a rupture disk where the flow is regulated by the entire relief line.

Figure 5: Body bowl choking for a gas system with a discharge line

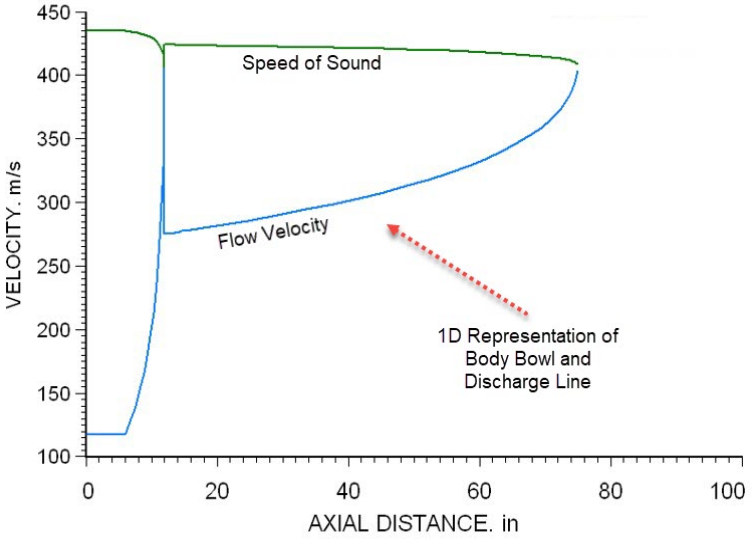

Source: Process Safety Office® SuperChems

In Figure 6 we add an expander to the PRV outlet flange to enlarge the diameter of the discharge line. We notice that we now have three choke locations: (a) one choke at the PRV nozzle, (b) one choke at the PRV body bowl, and (c) one choke at the end of the discharge line. The first choke regulates the flow, the second choke regulates the backpressure to the PRV and the third choke regulates the end of pipe exit pressure.

8 Body Bowl Choking in Twophase Systems

The same body bowl choking can occur in two phase flow with added complexities due to phase change, non-equilibrium flow, and slip between the two phases. The choke point and conditions are highly influenced by the initial vapor quality. Body bowl choking can be more severe for for slightly subcooled flow or flows with low levels of inlet vapor content (see Figure 7). The difference between equilibrium and non-equilibrium nozzle flow becomes less important as the inlet vapor content or quality increases [19, 20, 18].

For twophase flow, homogeneous equilibrium flow results in higher body bowl choking pressures than slip

Figure 6: Body bowl choking for a gas system with an expander and a discharge line

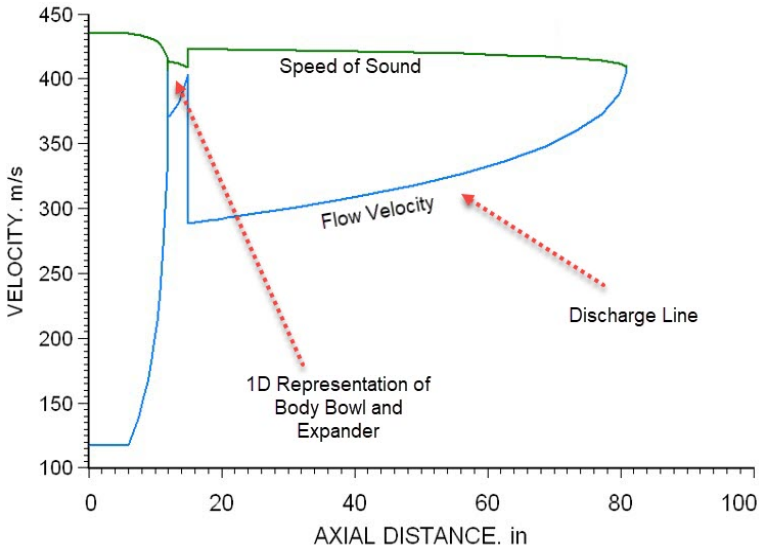

Source: Process Safety Office® SuperChems

equilibrium flow as demonstrated by Huff [18]. This high level of body bowl pressure for homogeneous equilibrium flow may be unreasonably restrictive. Operating experience with twophase flow systems indicates that slip equilibrium occurs is the body bowl and discharge line.

The considerations discussed above make it practically impossible to account for body bowl choking in twophase flow systems without the aid of a computer code such as Process Safety Office® SuperChems.

Figure 7: Body bowl back pressure limitation vs. inlet vapor quality at 10 % overpressure for steam/water system

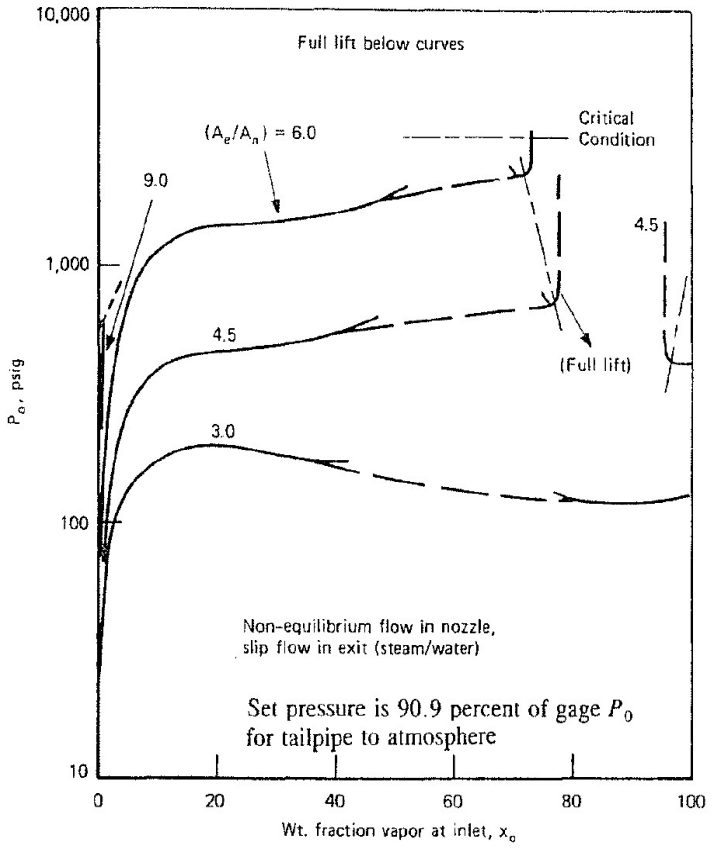

Source: [18]

9 Multiple Chokes

Discharge piping with flow area changes (expansions) can be subjected to multiple chokes for gas and twophase flow.

Temperatures associated with pressure discontinuities in the discharge line cannot be properly calculated for gas/vapor flow using an ω like method [21, 22, 23] because the thermodynamic path for a discontinuity is different than the thermodynamic flow path for a nozzle. Temperature values can be bounded however, by producing two sets of calculations with bounding thermodynamic flow paths, isentropic and isenthalpic (constant stagnation enthalpy). Temperature values associated with pressure discontinuities are reasonably represented by generalized reduced analytical models as long as the flow is twophase.

The identification of multiple chokes [24] for steady state flow requires complex iterative calculations and resolution of irreversible shock discontinuities. If the starting pressure is high enough, multiple chokes can occur in relief line downstream piping. Multiple chokes in relief piping should be avoided because they increase acoustic induced vibration failure risks. The identification and location of multiple chokes as well as the resolution of shock discontinuities are implicit in the 1D numerical solution of the gas dynamics equations (see Section 6.1).

10 Valve Closure Time and Pressure Surges

A widely studied problem in the fluid mechanics literature is water hammer. Rapid closure of valves causes pressure surges upstream of the valve which can be very damaging to piping systems and piping supports. For PRV's chattering in liquid service, a similar problem occurs when the PRV closes rapidly. Data reported by API on incidents involving PRVs in liquid service support this assertion. Water hammer is manifested as series of shocks, sounding like hammer strikes, which may have sufficient magnitude to rupture pipes or damage connected equipment. The excess pressure due to water hammer is additive to the normal flow pressure in the pipe.

The coupled solution of fluid hydraulics and timed valve closure is very similar to the PRV stability analysis in liquid service. Instead of the valves closing over a specified time, the PRV will close and open based on a force balance around the valve disk. Since liquid flows are rarely choked, the PRV stability solution is simpler than choked gas and/or multiphase flow. We will first solve the timed valve closure problem and then the PRV stability problem, since there are a lot of similarities and essentially the same boundary conditions for the inlet line.

Figure 8: Moody's Waterhammer Solution

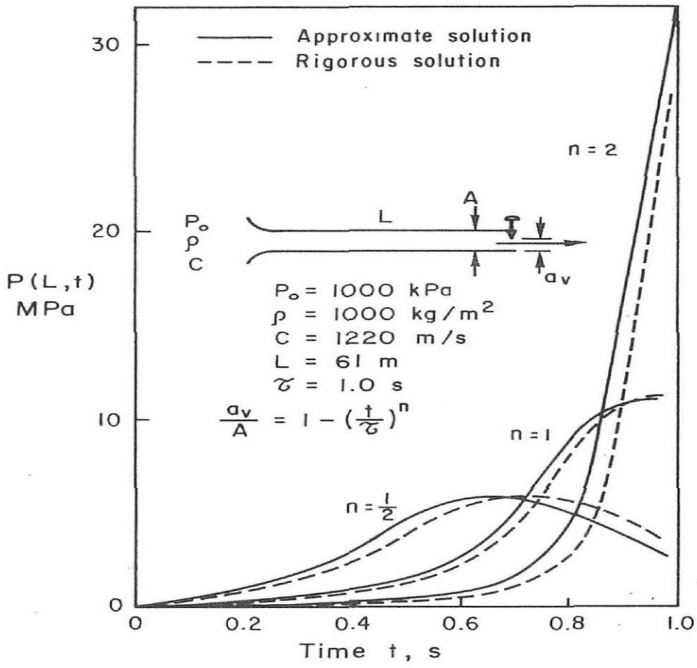

Time dependent valve closure is typically expressed using a simple model which relates the valve flow area as a function of pipe flow area:

$$\frac{A_v C_{d,v}}{A_P} = \beta = 1 - \left(\frac{t}{t_v}\right)^n \tag{91}$$

where t_v is the valve closure time and n is a exponent typically set at 0.5, 1, or 2 depending on the valve closure linearity.

PRV valve opening/closing and flow area are addressed by the single degree of freedom model developed earlier in this document. PRV flow area depends a several parameters including pressure at the valve disk surface, backpressure, spring constant, and damping.

Since we are solving this problem for an incompressible fluid, we will assume a constant density fluid and only need to solve the following two partial differential equations for pressure and

velocity:

$$\frac{\partial u}{\partial t} = -u\frac{\partial u}{\partial x} - \frac{1}{\rho}\frac{\partial P}{\partial x} - g\underbrace{\frac{\partial z}{\partial x}}_{\sin\theta} - \frac{2fu|u|}{D} - \frac{1}{2}u|u|\frac{K}{L} \tag{92}$$

$$\frac{\partial P}{\partial t} = -\frac{\rho u c^2}{A}\frac{\partial A}{\partial x} - uc^2\frac{\partial \rho}{\partial x} - \rho c^2\frac{\partial u}{\partial x} \tag{93}$$

where K is the number of velocity heads associated with pipe fittings. The above equations are developed from the momentum and energy balances without heat exchange and work. The term $c^2\frac{\partial \rho}{\partial x}$ in the pressure explicit energy equation is equal to $\frac{\partial P}{\partial x}$ which leads to the simplified pressure equation above. Many literature publications report these equations for constant flow area without elevation changes and ignore the change of velocity with axial distance for the momentum equation as well to yield:

$$\frac{\partial u}{\partial t} = -\frac{1}{\rho}\frac{\partial P}{\partial x} - \frac{2fu|u|}{D} \tag{94}$$

$$\frac{\partial P}{\partial t} = -\rho c^2\frac{\partial u}{\partial x} \tag{95}$$

All liquids are slightly compressible. For isothermal liquid flow, the change of liquid density with respect to axial distance can be related to the change of pressure if a reference isothermal compressibility factor is provided:

$$\kappa_T = \frac{1}{\rho}\left[\frac{\partial \rho}{\partial P}\right]_T \tag{96}$$

$$\frac{\rho}{\rho_o} \simeq 1 + \kappa_T\left(P - P_o\right) \tag{97}$$

$$\frac{\partial \rho}{\partial x} \simeq \rho_o\kappa_T\frac{\partial P}{\partial x} \tag{98}$$

As a result,

$$\frac{\partial P}{\partial t} = -\frac{\rho u c^2}{A}\frac{\partial A}{\partial x} - uc^2\rho_o\kappa_T\frac{\partial P}{\partial x} - \rho c^2\frac{\partial u}{\partial x} \tag{99}$$

The flow boundary condition can be defined as follows for the valve discharge side:

$$\frac{\partial u}{\partial x} = 0 \tag{100}$$

$$P = P_b + \frac{1}{2}K_v u^2\rho \tag{101}$$

$$K_v \simeq \left(\frac{1}{\beta} - 1\right)^2 \text{ where the velocity is the pipe velocity, or} \tag{102}$$

$$K_v \simeq \left(1 - \beta\right)^2 \text{ where the velocity is at the vena-contracta of the flow element, or} \tag{103}$$

$$\tag{104}$$

For the upstream pressure source side, the boundary conditions are defined as:

$$\frac{\partial P}{\partial t} = 0 = -\rho c^2 \frac{\partial u}{\partial x} - \frac{u\rho c^2}{A}\frac{\partial A}{\partial x} - u\frac{\partial P}{\partial x} \tag{105}$$

$$P_0 = P + \frac{1}{2}\rho u^2 \tag{106}$$

Note that $\frac{\partial P}{\partial x} = c^2 \frac{\partial \rho}{\partial x}$ for isentropic flow (see Equation 73).

The numerical solution of the partial differential equations for velocity and pressure often require some form of artificial dissipation (viscosity) to ensure stability of the solution:

$$\frac{\partial u}{\partial t} = \nu_u \frac{\partial^2 u}{\partial x^2} - u\frac{\partial u}{\partial x} - \frac{1}{\rho}\frac{\partial P}{\partial x} - g\underbrace{\frac{\partial z}{\partial x}}_{\sin\theta} - \frac{2fu|u|}{D} - \frac{1}{2}u|u|\frac{K}{L} \tag{107}$$

$$\frac{\partial P}{\partial t} = \nu_P \frac{\partial^2 P}{\partial x^2} - \frac{\rho u c^2}{A}\frac{\partial A}{\partial x} - uc^2\rho_o\kappa_T\frac{\partial P}{\partial x} - \rho c^2\frac{\partial u}{\partial x} \tag{108}$$

where ν_u and ν_P are on the order of:

$$\nu_u \sim \Delta x|u| \tag{109}$$

$$\nu_P \sim \Delta x\frac{c^2}{|u|} \tag{110}$$

$$\tag{111}$$

where Δx is the finite difference step size used for the discretization of the flow path length. As $\Delta x \to 0$, both $\nu_u \to 0$ and $\nu_P \to 0$. In some instances and depending on the solution method, the time step may be restricted to be less than or equal to the convection time step at every grid point:

$$\Delta t\left(\frac{|u| + c}{\Delta x}\right) \leq 1 \tag{112}$$

For two dimensional solutions:

$$\Delta t\left(\frac{|u_x| + c}{\Delta x} + \frac{|u_y| + c}{\Delta y}\right) \leq 1 \tag{113}$$

10.1 Liquid Pressure at Closing Valve

We apply the valve closure solution to a problem defined by Moody [12]. A straight, uniform, frictionless pipe of length L = 61 m is attached by an ideal nozzle to a vessel at pressure P_0 = 1000 kPa. Liquid of density $\rho = 1000\ \mathrm{kg/m^3}$ and sound speed c = 1220 m/s flows steadily through the pipe where it is discharged to zero ambient pressure. A valve at the discharge end closes with a

Figure 9: Moody's Waterhammer Solution Reproduced with SuperChems Expert v7.23

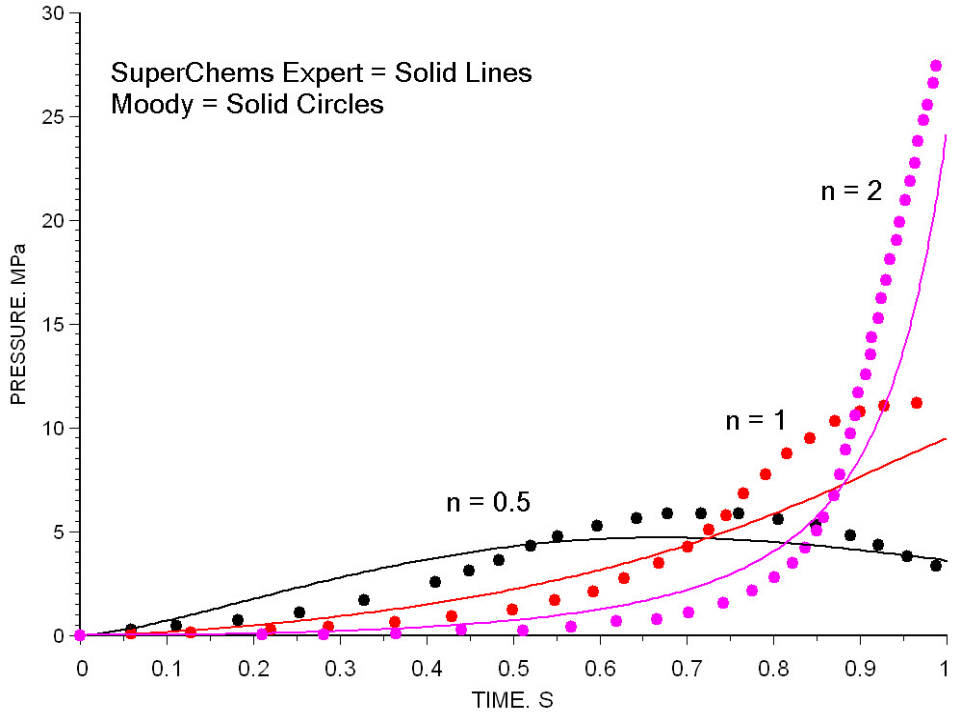

valve-to-pipe area ratio defined earlier. Determine the pressure as a function of time just upstream from the valve for a closure time $t_v = 1.0$ s and values of n = 0.5, 1.0, and 2.0. Assume that the valve flow discharge coefficient is 1.

The maximum pressure expected at the valve is:

$$u = \sqrt{\frac{2P_0}{\rho}} = \sqrt{\frac{2 \times 10^6}{1000}} = 44.72\,\mathrm{m/s} \tag{114}$$

$$P_v = uc\rho = 44.72 \times 1220 \times 1000 = 54.55\,\mathrm{MPa} \tag{115}$$

Figure 8 provides the solution provided by Moody. Note the peak pressure realized at the valve is less than the predicted maximum value of 54.55 MPa and depends on the how fast the valve is closing. With a power exponent of 2, most of the reduction in valve flow area occurs towards the end of the closure time. This solution was produced assuming zero pressure loss due to friction. The resulting dynamic force loads on the valve and upstream piping can be very large if the pipe diameter is large. Piping and valve damage potential increases with pipe diameter for valves in liquid service.

We reproduced Moody's frictionless solution using SuperChems Expert (a component of Process Safety Office®) as shown in Figure 9. Reasonable agreement is obtained.

If we assume a pipe diameter of 8 inches and allow pressure loss due to friction, we can continue the solution beyond the valve closure and produce an estimate of the pressure profiles in the pipe as the pressure wave bounces back and forth from the source to the closed valve.

Figure 10: SuperChems Expert v7.23 Waterhammer Solution at n = 1 with Friction

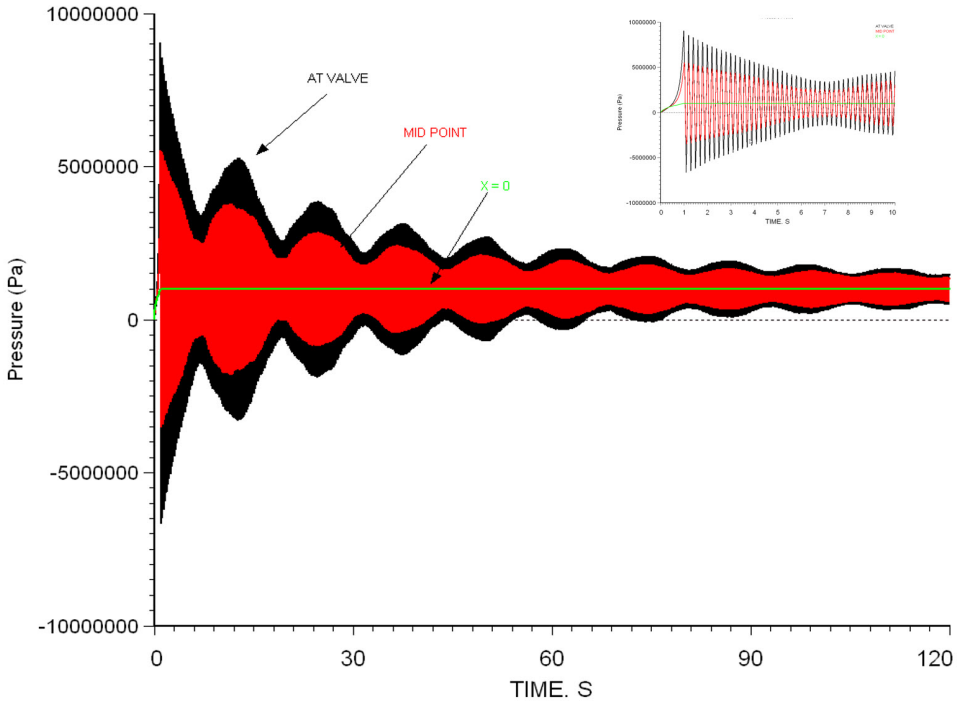

We will extend this analysis later on in this document to PRV installations in liquid, gas, and two-phase service.

10.2 Singh and Shak Estimate of ΔP_{total}

For simple piping configurations (constant diameter piping without area changes and/or the presence of other acoustic barriers) the upstream pressure drop or rise during the PRV opening or closing (linear behavior assumed by Singh and Shak) can be estimated from the following equations:

$$
\begin{aligned}
t_{wave} &= \frac{2L_p}{c_0} \\
\tau &= \min\left(\frac{t_{wave}}{t_{valve}}, 1\right) \\
\Delta P_{wave} &= \underbrace{\tau \frac{c_0 \dot{M}}{A_p}}_{\text{Fluid Hammer Term}} + \underbrace{\tau^2 \frac{\dot{M}^2}{2\rho_0 A_p^2}}_{\text{Fluid Inertia Term}} \qquad 0 \le \tau \le 1 \qquad (116) \\
\Delta P_{wave} &= \tau \rho u c_0 \left[1 + \frac{\tau \rho u}{2\rho_0 c_0}\right] \qquad 0 \le \tau \le 1 \qquad (117)
\end{aligned}
$$

where the subscript 0 indicates upstream vessel conditions, $\dot{M}$ is the mass flow rate at full PRV open position, and t_{valve} is the PRV opening or closing time. The fluid inertia term in ΔP_{wave} is

normally small but becomes important for high speed flow where the pressure drop is severe and excessive. For an ideal gas, the isentropic speed of sound $c_0 = \sqrt{\gamma \frac{P_0}{\rho_0}}$.Equation 117 is based on the acoustic wave theory where the valve opening or closing is assumed to be instantaneous. Singh and Shak [9] recommend the use of the steady state value of $\dot{M}$ as a conservative value. Similarly, the pressure drop due to friction during opening or closing of the PRV can be estimated from the steady state value and τ:

$$\Delta P_{f,wave} = \tau^2 \Delta P_f = \tau^2 \frac{\dot{M}^2 \left(K + \frac{4 f L_p}{D_p} \right)}{2 \rho_0 A_p^2} \quad 0 \leq \tau \leq 1 \tag{118}$$

where K is the number of velocity heads loss, f is the Fanning friction factor, D_p is the pipe diameter, and L_p is the pipe length. If the actual piping configuration is complex, one or two-dimensional fluid dynamics equations solutions may be required to estimate the acoustic pressure drop due to expansion and reflections of the pressure wave.

If we use Singh and Shak's equation to estimate ΔP_{wave} using a valve exponent of 0.5 (close to linear behavior), we calculate a value that is very close to what is predicted using the dynamic water hammer solution:

$$\begin{aligned} t_{wave} &= \frac{2 L_p}{c_0} = \frac{2 \times 61}{1220} = 0.1 \\ \Delta P_{wave} &= \tau \rho u c_0 \left[1 + \frac{\tau \rho u}{2 \rho_0 c_0} \right] = 5.455 \times \left[1 + \frac{0.1 \times 44.72}{2 \times 1220} \right] = 5.5 \, \text{MPa} \end{aligned} \tag{119}$$

The ΔP_{wave} equation proposed by Singh and Shak can be used to approximate the total pressure drop in the inlet relief line of a PRV installation as long as the inlet relief line geometry is simple. Once the valve is closed the calculated round trip travel time by the partial differential equations solution of the pressure wave is 0.2 seconds, or:

$$\Delta t = \frac{4L}{c_0} = \frac{4 \times 61}{1220} = 0.2 \text{ s} \tag{120}$$

This is shown in Figure 10 in the expanded pressure-time profile which shows approximately 5 round trips for the pressure wave in 1 second once the valve is closed.

The equation provided by Singh and Shak is attributed to Joukowsky [25]. In 1898 Joukowsky was the first one to show the validity of the wave pressure drop equation. He experimented with the effect of slow valve closure times and concluded that when the valve closure time is longer than the round trip time of the pressure wave, the excess pressure is reduced in intensity according the the proportion:

$$\frac{\Delta P_{wave}}{\Delta P_{wave,max}} = \frac{2L}{t_{valve} c_0} = \tau \tag{121}$$

We note that the original Joukowsky [25] equation did not address transient cavitation and liquid column separation, line packing, and piping systems reflections caused by piping components, pressure relief devices, flow area changes, and surge suppression devices [26].

Cavitation can occur when the downsurge pressure (negative transient pressure wave) causes the liquid pressure to drop below its vapor pressure leading to vapor generation. Liquid column separation occurs when enough vapor is generated to occupy the entire pipe cross sectional area. The subsequent collapse of the vapor during an upsurge (positive transient pressure wave) can cause a much higher pressure increase than what is predicted by the Joukowsky equation.

Line packing occurs when the sudden closure of a valve causes the propagation of a pressure wave (water hammer) inside the pipe but fails to bring the entire fluid body to a zero velocity except at the location of the closed valve. The fluid behind the initial water hammer pressure wave still has forward velocity towards the valve. As a result, the pressure at the valve continues to increase slowly in excess of the Joukowsky pressure. In this case, line packing can cause irrecoverable frictional pressure loss (assuming that the fluid is always flowing) to be recovered (since the fluid is no longer flowing). Line packing becomes significant for long pipelines with low viscosity fluids or where frictional pressure drop is significant in relatively short pipe systems due to the presence of highly viscous fluids for example.

Pressure wave reflection typically occurs where flow area and/or flow direction changes occur. In these cases both a reflected pressure wave and a transmitted pressure wave will occur at the transition point [26].

11 Considerations for Low Compressibility Fluids

High frequency (rapid) PRV cycling and instability (fluttering or chattering) in liquid systems or high pressure gas systems will often require mitigation because the resulting pressure transients can cause severe damage to the relief piping and its components including the PRV itself. PRV instability is most important for liquid systems. Historically, more severe damage is reported to occur to relief and piping systems in liquid service.

The opening or closing of a pressure relief device can create unacceptable pressure conditions in the relief inlet and/or discharge piping that are either too high (upsurge) or too low (downsurge). This is especially pronounced in liquid systems. The pressure transients are caused by the rapidly changing flow rates during the opening or closing of the pressure relief device. Significant pressure transients can cause component failures and leaks as well as PRV chatter, PRV damage, and liquid column separation.

During rapid PRV opening, the pressure upstream of the PRV attempts to drop by the Joukowski pressure change, and the associated downsurge is propagated to the upstream pressure source/vessel. Similarly, as the PRV closes rapidly, a lower pressure is created downstream of the PRV and a downsurge is propagated to the downstream piping. During PRV closing, and as the flow velocity is decreasing at the PRV, a reflected pressure wave or upsurge is propagated back to the source. This upsurge is significant for liquid as the flow is arrested and the dynamic pressure is converted into stagnation pressure. Pressure transients can cause severe damage, especially in where the relief piping is initially liquid full or packed.

During the low pressure transient or downsurge caused by the rapid relief device opening, the pressure can fall below the vapor pressure of the liquid causing vapor formation (cavitation). The

vaporization of the liquid divides the liquid column into distinct columns. As a result, two phase flow can occur. The vapor cavity (bubbles) continue to grow until a higher pressure develops as the relief device recloses. Rapid pressure rise will then occur following the collapse of the recently created vapor during this recurring high pressure transient which can cause severe and destructive surges as well as noise and vibrations when the liquid column rejoins.

In addition, the rapid evolution of dissolved gases from a flowing liquid during downsurge can lead to increased speed of sound for that liquid. Because gas dissolution is slower during the upsurge cycle, it is challenging to get an accurate estimate of the effective speed of sound for the pipe/fluid system. Hos et al. [6] recently reported an effective speed of sound for the water/piping system used in testing PRV stability for liquids of 857 m/s. This lower value is mostly due to the impact of dissolved air in water and is substantially lower that they typical value of 1430 m/s.

An effective solution to prevent severe pressure transients is to use a relatively slower PRV. A friction damper has been used successfully in Europe to slow down the PRV opening and closing. BASF initially proposed this concept.

A shorter inlet relief line can also reduce the magnitude or pressure transients because if the inlet line is short enough, the returning pressure wave from the source after the initial downsurge cause by PRV opening can help to keep the PRV from closing further and to stay open.

Using a larger inlet line diameter also works but may be impractical and cost prohibitive for existing installations. The risks associated with cutting new vessel nozzles, replacement of piping and supports, shutdowns and restarts of plant units to effect this type of mitigation may not be desirable.

Increasing the inlet line diameter changes the liquid velocity for a given PRV flow rate. When the inlet pipe diameter is increased, the resulting reduction in flow velocity decreases the magnitude of the initial pressure wave during opening (downsurge) and can prevent cavitation from occurring all together.

Finally, Pipe re-enforcements (higher ratings), changing the piping supports, material of construction, etc. are also possible mitigation measures that can be considered for fluttering and/or rapid cycling in liquid systems or high pressure gas systems.

The same effect can be achieved by using a small high pressure surge tank or vessel. One way surge vessels can be an effective mean of preventing the downsurge during PRV opening and can ensure that the PRV remains open by admitting high pressure fluid (for example high pressure nitrogen) into the inlet piping during PRV opening to keep the PRV open during the downsurge transient.

The presence of a vapor/gas pocket/volume can act as a surge absorber and can reduce the magnitude of the peak pressure reached due to deceleration of the liquid by converting the liquid kinetic energy into adiabatic compression of the gas/vapor pocket or volume. For a pipe of length L, flow diameter D, and for a liquid volumetric flow rate of $\dot{v}_l$ the total kinetic energy is:

$$\text{Kinetic Energy} = 2\frac{\rho L \dot{v_l}^2}{\pi D^2} = \frac{1}{2} m u_l^2 \tag{122}$$

If we convert the total kinetic energy of the liquid when the liquid is stopped to adiabatic compres-

sion work done on the vapor/gas, we obtain:

$$-2\frac{\rho L \dot{v_l}^2}{\pi D^2} = \int_{v_{g,1}}^{v_{g,2}} P(v_g) dv_g \tag{123}$$

For an ideal gas:

$$-2\frac{\rho L \dot{v_l}^2}{\pi D^2} = \frac{v_{g,1}\left(P_1 - P_2\left[\frac{P_1}{P_2}\right]^{1/\gamma}\right)}{\gamma - 1} \tag{124}$$

The above equation can be solved for $v_{g,1}$ such that the final pressure spike P_2 does not exceed a specific limit. This is how gas filled surge absorbers are typically designed. A safety margin of 10 % is typically added to $v_{g,1}$:

$$v_{g,1} \simeq \frac{\left(-2\frac{\rho L \dot{v_l}^2}{\pi D^2}\right)(\gamma - 1)}{0.9\left(P_1 - P_2\left[\frac{P_1}{P_2}\right]^{1/\gamma}\right)} \tag{125}$$

12 Impact of Pipe Junctions on Pressure Waves

Transient pipe flow results from the generation and propagation/reflection of pressure waves that occur as the result of disturbance in the pipe/fluid system. Typical pipe/fluid disturbances include the closure or opening of a valve, the actuation of a relief device, the start or trip of a pump, etc. A pressure wave, which represents a rapid pressure and associated flow change (the unbalanced pressure causes the fluid to accelerate), travels at the speed of sound of the fluid-pipe system. The pressure wave is partially transmitted and reflected at all discontinuities in the piping system. Discontinuities include pipe junctions, pumps, open or closed pipe ends, surge tanks, etc.

The magnitude of pressure waves that are transmitted and reflected from piping junctions can be calculated if conservation of mass and momentum are enforced [27]. Although this approach neglects the small amount of energy losses associated with the junction geometry, the impact on the actual pressure wave values is minimal.

Figure 11 illustrates the impact of a pressure wave of magnitude ΔP_{wave} impinging on one of the legs, $i = 1$, that is equally transmitted to each of the adjoining legs equally. The magnitude of the transmitted pressure wave is $T_i \Delta P_{wave}$ where the transmission coefficient T_i is given by:

$$F_i = \frac{c_i}{g A_i} \tag{126}$$

$$T_i = \frac{\frac{2}{F_i}}{\sum_j \frac{1}{F_j}} \tag{127}$$

$$R_i = T_i - 1 \tag{128}$$

Figure 11: Impact of pipe junctions on pressure waves

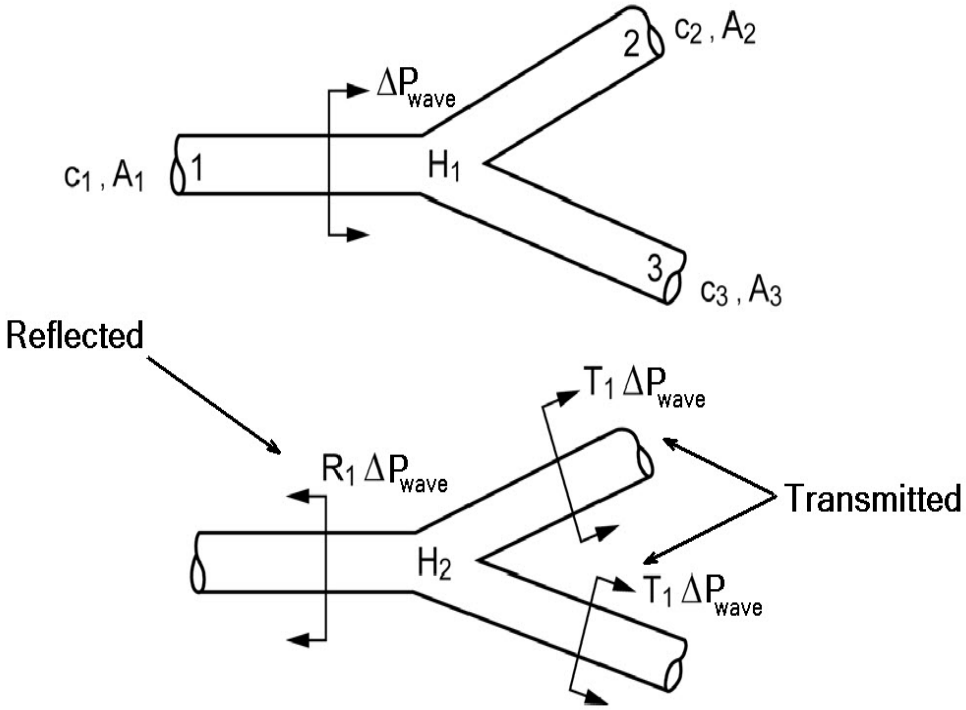

where g is the acceleration due to gravity, c_i is the effective speed of sound in leg i, R_i is the reflected pressure wave coefficient in leg i, and j is the summation index of all the legs connecting at the junction. R_i can be positive or negative. For the junction illustrated in Figure 11:

$$T_1 = \frac{\frac{2gA_1}{c_1}}{\frac{gA_1}{c_1} + \frac{gA_2}{c_2} + \frac{gA_3}{c_3}} \tag{129}$$

$$R_1 = T_1 - 1 \tag{130}$$

For a pipe junction where the flow splits from one leg with flow area A_1 into two pipes with flow areas that are each equal to A_1 and where the effective speed of sound of the pipe/fluid system are equal in all three legs, the transmission coefficient will be equal to 2/3 and the reflected pressure coefficient will be -1/3:

$$T_1 = \frac{\frac{2gA_1}{c_1}}{\frac{gA_1}{c_1} + \frac{gA_1}{c_1} + \frac{gA_1}{c_1}} = \frac{2}{3} \tag{131}$$

$$R_1 = T_1 - 1 = \frac{2}{3} - 1 = -\frac{1}{3} \tag{132}$$

Equation 127 applies to the simple cases of a dead end junction and an open end junction such as a connection to a large reservoir or tank. In the case of a dead end junction, this would qualify as a two-pipe junction system with $A_2 = 0$ which leads to:

$$T_1 = \frac{\frac{2gA_1}{c_1}}{\frac{gA_1}{c_1} + 0} = 2 \tag{133}$$

$$R_1 = T_1 - 1 = 2 - 1 = 1 \tag{134}$$

An R_1 value of 1 indicates that the pressure wave is reflected positively. In the case of a open connection to a large reservoir, $A_2 = \infty$ we obtain:

$$T_1 = \frac{\frac{2gA_1}{c_1}}{\frac{gA_1}{c_1} + \infty} = 0 \tag{135}$$

$$R_1 = T_1 - 1 = 0 - 1 = -1 \tag{136}$$

An R_1 value of -1 indicates that a negative pressure wave reflection occurs at the reservoir.

13 Speed of Sound Estimates

The speed of sound values used in the estimation of wave travel time can be subject to uncertainty. This is most important for liquids and two-phase systems. The piping flexibility can lower the value of the speed of sound. The presence of small amounts of entrained gas in liquids can also reduce the speed of sound. Adding a small amount of gas to a liquid, say 0.1 % by volume can lower the speed of sound for the two-phase mixture by a factor of two.

For rigid piping, the speed of sound is equal to the fluid speed of sound:

$$c = c_0 = \sqrt{\frac{1}{\kappa_S \rho}} \tag{137}$$

where κ_S is the isentropic compressibility.

For piping that is anchored against longitudinal movement throughout its length:

$$c = c_0 \eta = \frac{c_0}{\sqrt{1 + \frac{E_f}{E_s}\frac{d}{\delta}(1 - \nu^2)}} \tag{138}$$

Where $E_f = \frac{1}{\kappa_T}$ is the fluid isothermal bulk modulus of elasticity [4] in Pa, E_s is the pipe material of construction modulus of elasticity in Pa, d/δ is the piping diameter to thickness ratio, and ν is Poisson's ratio ($\simeq 0.3$).

[4] The adiabatic bulk modulus of elasticity can also be used. $E_f = \frac{1}{\frac{C_p}{C_v}\kappa_T}$

Table 1: Impact of piping flexibility on speed of sound reduction

Material	Piping Schedule US	E_f, GPa	$\frac{d}{\delta}$	η
Liquid Water	5	2.19	52.2	0.799
Liquid Water	10	2.19	35.5	0.850
Liquid Water	40	2.19	13.4	0.934
Liquid Water	80	2.19	11.3	0.944
Liquid Water	160	2.19	6.47	0.967
Liquid Propane	5	0.11	52.2	0.986
Liquid Propane	10	0.11	35.5	0.991
Liquid Propane	40	0.11	13.4	0.996
Liquid Propane	80	0.11	11.3	0.997
Liquid Propane	160	0.11	6.47	0.998
Vapor Propane	5	6.8×10^{-4}	52.2	1.000
Vapor Propane	10	6.8×10^{-4}	35.5	1.000
Vapor Propane	40	6.8×10^{-4}	13.4	1.000
Vapor Propane	80	6.8×10^{-4}	11.3	1.000
Vapor Propane	160	6.8×10^{-4}	6.47	1.000

Propane data at 293 K and 8.35 bara

For piping anchored against longitudinal movement at the upper end:

$$c = c_0\eta = \frac{c_0}{\sqrt{1+\frac{E_f}{E_s}\frac{d}{\delta}\left(1.25-\nu\right)}} \tag{139}$$

For piping where frequent expansion joints are present:

$$c = c_0\eta = \frac{c_0}{\sqrt{1+\frac{E_f}{E_s}\frac{d}{\delta}}} \tag{140}$$

The impact of piping flexibility on speed of sound estimates is illustrated in Table 1 for steel piping with frequent expansion joints. The speed of sound reduction is most important for liquids that are highly incompressible where thin wall piping is used.

14 Izuchi Estimate of ΔP_{total}

In his published work Izuchi [2, 3] couples the inlet pipe dynamics with a single degree of freedom valve model. He divides the relief piping into discrete volumes and uses a interpolating scheme for velocity to solve the fluid dynamics equations. In addition, he writes balances for the PRV body bowl which provides a direct value of the backpressure on the valve disk. Variable flow area was not addressed in his model. Izuchi's solution was later replicated by Pentair [4].

15 Boundary Conditions

The boundary conditions are critically important for coupling the pressure source and the PRV inlet line. Boundary conditions are also needed for the discharge side of the PRV. Both Izuchi [2] and Pentair [4] use stagnation enthalpy boundary conditions. Although our solution for the vessel balances are far more detailed, we use similar boundary conditions.

The pipe flow dynamics are solved for velocity, temperature, and density directly and indirectly for pressure using Equations 39, 61, 47, and pressure 65. The pressure change with respect to axial distance is represented in terms of density and temperature:

$$\frac{\partial P}{\partial x} = \frac{R_g}{M_w}\left[T\frac{\partial \rho}{\partial x} + \rho\frac{\partial T}{\partial x}\right] \tag{141}$$

We therefore need three boundary conditions for coupling the pressure source to the inlet line:

$$h_0 = h + \frac{1}{2}u^2 \tag{142}$$

$$s_0 = s \tag{143}$$

$$\left[\frac{\partial P}{\partial t}\right]_0 = \left[\frac{\partial P}{\partial t}\right] \tag{144}$$

Another three boundary conditions are required to couple the inlet pipe end conditions to the PRV inlet conditions:

$$uA\rho = C_d A_v u_v \rho_v \tag{145}$$

$$h = h + \frac{1}{2}u_v^2 \tag{146}$$

$$\left[\frac{\partial P}{\partial t}\right] = \left[\frac{\partial P}{\partial t}\right]_v \tag{147}$$

where u_v can be estimated using choked or subsonic flow.

16 Estimation of PRV Parameters

Part II of this paper [28] includes a detailed description of how to estimate the PRV spring constant K_s and weight in motion m_D as well as PRV opening and closing times semi-empirical formulas.

17 Cycles to Failure

It is expected that valves in high pressure and/liquid service have the most damage potential, especially when the valve size is large. Large fluid and mechanical forces are associated with large valves.

18 Force vs. Lift Data and the Steady State Disk Force Balance

The disk lift parameters α, η, θ_o, and ψ have to be established using test data. In the absence of test data, these parameters can be estimated from a manufacturer supplied K_b or K_w curve or flow test data at different overpressure values where flow occurs at reduced lift.

18.1 Flow Angle and Blowdown Relationship

Assuming steady state and stable operation at reduced lift, Equation 17 can be solved to establish the value of either η, ω, and/or θ_0 for the disk force balance model. The disk force balance model has to be consistent with the actual pressure relief valve blowdown. If multiple data points are available, η, ω, and/or θ_0 can be regressed for best fit of all the available data. Such data can be obtained from manufacturers reported k_b or k_w data for specific valve models at one or more flow overpressures, typically for air and water.

$$
\begin{aligned}
F_{NET} \;=\; & \underbrace{P_I A_I + \eta P_* \left(A_D - A_I\right) + \frac{G^2 A_c^2}{\rho_I A_I}}_{F_{Up,1}} + \underbrace{\left[\frac{G^2 A_c^2}{2\pi R_1 x C_d \rho_e}\right]}_{F_{Up,2}} \cos\theta \\
& - \left[\underbrace{P_B A_D + K_s x + K_{sb} x + \left(P_{atm} - P_B\right) A_{bel} + \left(P_{set} - P_{atm}\right) A_I}_{F_{Dn}}\right]
\end{aligned}
\tag{148}
$$

where G is the mass flux, A_c is flow area limited by critical lift, ρ_e is the density at the curtain exit plane, and x is the disk lift which may be larger than the critical lift when the flow is choked at the nozzle. If the pressure relief valve is operating stably during steady state at a specific disk lift x, then $F_{NET} = 0$:

$$
\cos\theta \;=\; \frac{P_B A_D + K_s x + K_{sb} x + \left(P_{atm} - P_B\right) A_{bel} + \left(P_{set} - P_{atm}\right) A_I - P_I A_I - \eta P_* \left(A_D - A_I\right) - \frac{G^2 A_c^2}{\rho_I A_I}}{\frac{G^2 A_c^2}{2\pi R_1 x C_d \rho_e}}
\tag{149}
$$

Consider a typical balanced bellows valve with $A_I = A_N$, $A_D = 1.2A_N$ and $A_{bel} = 1.08A_N$, $\eta = 0.7$, $\psi = 0.9$. If we consider the case of liquid flow ($P^* = P_I$) where the valve is operating stably at critical lift ($x = x_c$) and 10 % overpressure ($P_I = 1.1P_{set} - 0.1P_{atm}$) with atmospheric

backpressure ($P_B = P_{atm}$), we can simply the equation used to solve for $\cos\theta$:

$$x_c = \frac{R_N}{2\psi} \tag{150}$$

$$A_c = C_{d,max} A_N \tag{151}$$

$$K_s \simeq \left(\frac{P_{fullflow}}{P_{set} - P_{atm}}\right)\left(\frac{A_{pop}}{A_N}\right)\left[\frac{(P_{set} - P_{atm})A_N}{x_{max}}\right] = 1.32\left[\frac{(P_{set} - P_{atm})A_N}{x_{max}}\right] \tag{152}$$

$$\cos\theta = \frac{K_s x_c + A_N\left[P_{set} - P_I - 0.2\eta P_I + 0.2P_{atm}\right] - C_{d,max}\frac{G^2 A_c}{\rho}}{\frac{G^2 A_c}{\rho}} \tag{153}$$

$$= \frac{K_s}{4.4\pi\psi C_{d,max} R_N\left(P_{set} - P_{atm}\right)} - \frac{0.254P_{set} - 0.314P_{atm}}{2.2C_{d,max}\left(P_{set} - P_{atm}\right)} - C_{d,max} \tag{154}$$

$$\simeq 0.33\frac{R_N}{x_{max} C_{d,max}} - \frac{0.11}{C_{d,max}} - C_{d,max} \tag{155}$$

For a 6Q8 with maximum lift of 0.029 m, $R_N = 0.0503$ m, and $C_{d,max} = 0.69$, $\cos\theta = -0.026$ or the flow angle θ at critical lift is 90 degrees.

If the valve is going to close when the blowdown pressure is reached, then $P_I = \left(1 - \frac{\%BD}{100}\right) P_{set} + \frac{\%BD}{100} P_{atm}$ and $x = 0$.

18.2 Backpressure Data

K_b and K_w curves are usually provided to correlate flow capacity reduction vs. backpressure. This is illustrated in Figures 12 and 13 reproduced from reference [29].

If a manufacturer K_b curve is available, we can obtain an approximate value for the parameters η, θ_o, and ψ by solving the steady state force balance provided earlier in Equation 17. We can equate the value of K_b at a specific value of overpressure and backpressure to the valve disk lift distance, x:

$$K_b = \frac{2\sqrt{\pi}x}{\sqrt{A_N}}\left(\frac{x}{x_{max}}\right)^{\psi} \tag{156}$$

Regardless of the value of ψ, when the valve achieves full lift, i.e. $K_b = 1$, the above equation yields a value of $x = x_{max}$:

$$x = \frac{1}{2}\sqrt{\frac{A_N}{\pi}} = \frac{R_N}{2} = x_{max} \tag{157}$$

With at least three distinct points from a manufacturers K_b curve less than 1.0, we can solve for η, θ_o and ψ using Equation 156. Those values are solved in conjunction with Equation 17 to produce optimal (least squares) values of η, θ_o, and ψ that will best reproduce the K_b curve. Note that the solution is not very sensitive to the value of ψ.

Figure 12: Measured capacity reduction factor for bellows valves

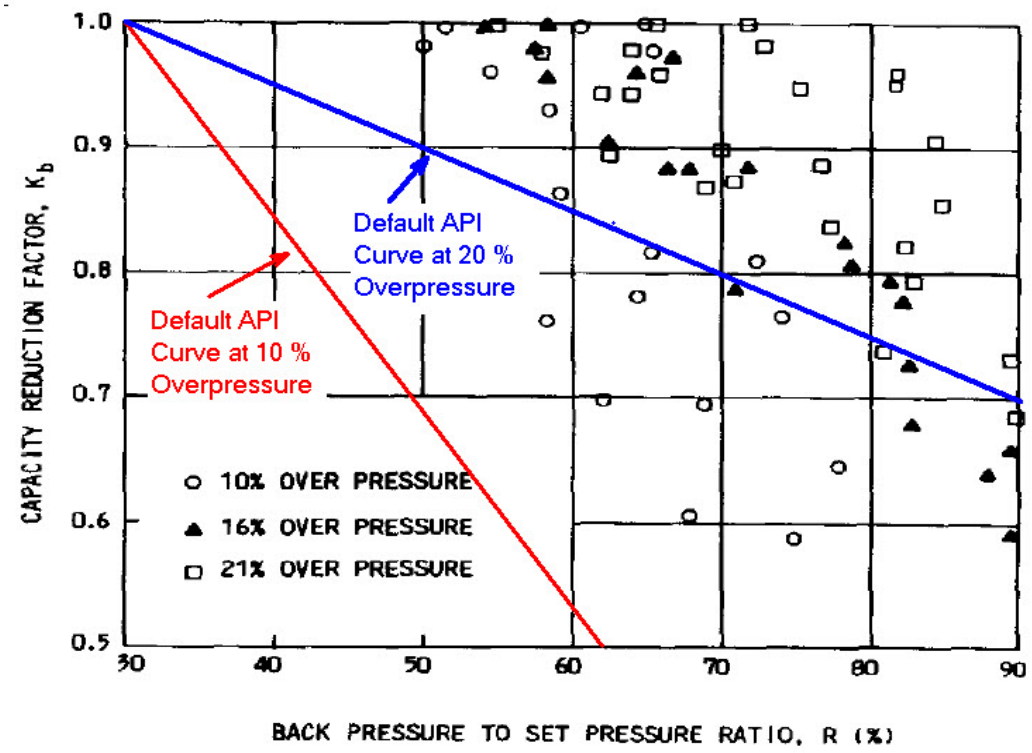

Figure 13: Measured capacity reduction factor for conventional valves

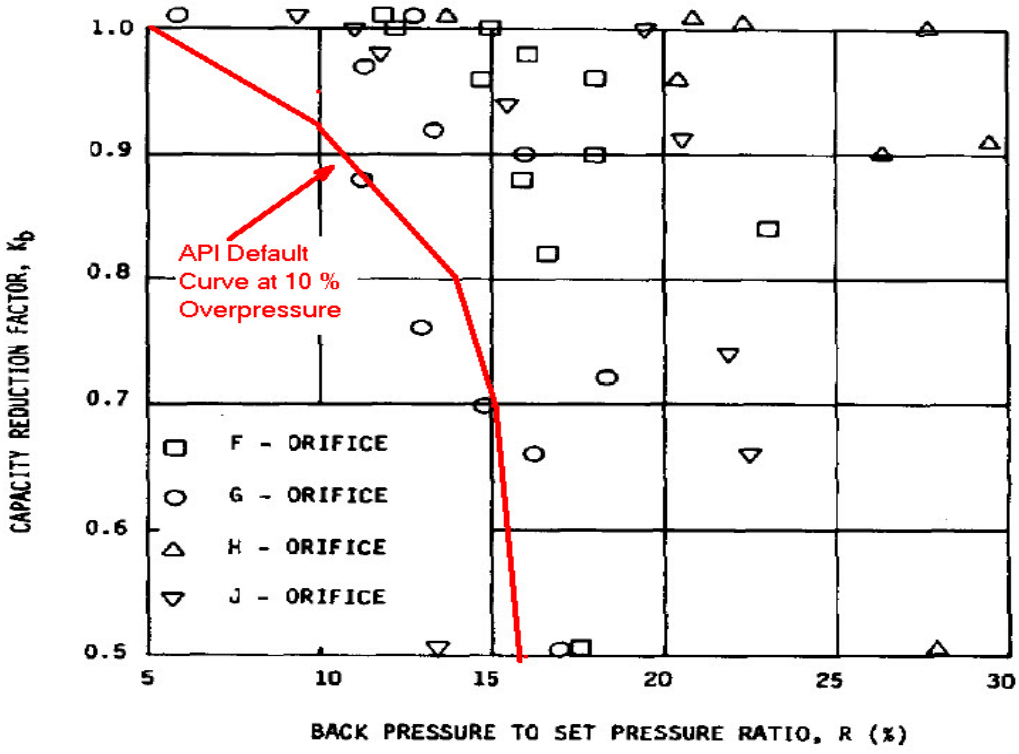

The equation system that needs to be solved for a single K_b point is summarized below for the case where $A_I = A_N$:

$$
\begin{aligned}
R_N &= \sqrt{\frac{A_N}{\pi}} && (158)\\
x_{max} &= \frac{R_N}{2} && (159)\\
x &= \frac{R_N}{2} K_b^{\frac{1}{1+\psi}} = x_{max} K_b^{\frac{1}{1+\psi}} && (160)\\
C_d &= C_{d,max} \left[\frac{x}{x_{max}}\right]^{\psi} = C_{d,max} K_b^{\frac{\psi}{1+\psi}} && (161)\\
A_D &\simeq 1.3 A_N && (162)\\
A_{bel} &\simeq 0.9 A_D \simeq 1.17 A_N && (163)\\
A_c &= 2x\sqrt{\pi A_N} \text{ where } x \leq \frac{R_N}{2} \leq x_{max} && (164)\\
\theta &= \theta_o \frac{x}{x_{max}} = \theta_o K_b^{\frac{1}{1+\psi}} && (165)\\
F_{NET} &= F_{Up} - F_{Dn} = 0 \\
&= \left(P_N - P_{set} + P_{atm}\right) A_N + \eta P_* \left(A_D - A_N\right) + \dot{m}^2 \left[\frac{\cos\theta}{A_c C_d \rho_e} + \frac{1}{\rho_N A_N}\right] \\
&\quad -P_B A_D - K_s x - K_{sb} x - \left(P_{atm} - P_B\right) A_{bel} && (166)
\end{aligned}
$$

Given at least three different K_b points from a manufacturer curve, we can solve numerically for the values of η, θ_o, and ψ that will minimize the sum of squares of the net force balance to yield the best fit of the three K_b values used. A perfect solution should result in a 0 value for the sum of squares of the net force balance from all three points. A preferred solution is to use multiple points at different overpressure levels, typically 10, 16, and 21 % and to regress the best set of parameters that can reproduce the entire K_b data sets represented by the manufacturer supplied curve(s).

We will illustrate the process for the specific case of a Consolidated balanced bellows 1900 series pressure relief valve (see [30]). Consolidated provides a K_b curve for gas/vapor flow as shown in Figure 14. Based on the data provided in [30] and in Figure 14 we can calculate the values of η, ψ, and θ_o that will best reproduce this data for all three curves, 10, 16, and 21 % overpressure:

$$
\begin{aligned}
P_{set} &= 185 \text{ psig} && (167)\\
R_N &= \sqrt{\frac{A_N}{\pi}} = \sqrt{\frac{12.347 \text{ in}^2}{\pi}} = 0.0504 \text{ m} && (168)\\
x_{max} &= \frac{R_N}{2} = 0.0252 \text{ m} && (169)\\
x &= \frac{R_N}{2} K_b^{\frac{1}{1+\psi}} = 0.0252 K_b^{\frac{1}{1+\psi}} && (170)\\
C_d &= C_{d,max}\left[\frac{x}{x_{max}}\right]^{\psi} = C_{d,max} K_b^{\frac{\psi}{1+\psi}} = 0.868 K_b^{\frac{\psi}{1+\psi}} && (171)\\
A_D &\simeq 1.2 A_N && (172)\\
A_{bel} &\simeq 0.9 A_D \simeq 1.08 A_N && (173)\\
A_c &= 2x\sqrt{\pi A_N} \text{ where } x \le \frac{R_N}{2} \le x_{max} && (174)\\
\dot{m} &= G A_c C_d && (175)\\
\theta &= \theta_o \frac{x}{x_{max}} && (176)\\
F_{NET} &= F_{Up} - F_{Dn} = 0 \\
&= \left(P_N - P_{set} + P_{atm}\right) A_N + \eta P_* \left(A_D - A_N\right) + \dot{m}^2 \left[\frac{\cos\theta}{A_c C_d \rho_e} + \frac{1}{\rho_N A_N}\right] \\
&\quad - P_B A_D - K_s x - K_{sb} x - \left(P_{atm} - P_B\right) A_{bel} && (177)
\end{aligned}
$$

The mass flux, density, and data required for the regression of the force balance variable parameters are shown in Table 2 for air. The regressed values resulting in the best fit regression are $\theta_o = 74.56$ degrees, $\psi = 0$, and $\eta = 0.591$ as shown in Figure 15. The regression confirms the linear dependence of θ on disk lift, a smaller angle with respect to vertical at lower lifts and larger angle as the valve goes into full lift. The regressed value of ψ of zero confirms the use of a constant discharge coefficient as previously suggested by Singh and Shak [9].

Once the parameters are known, one can exercise the force balance for any combination of inlet pressure and back pressure and can solve for the actual valve lift. We solve for the particular case where the inlet pressure at the disk surface is at $1.05 P_{set} = 175.75$ psig and a backpressure of 64.75 psig. We calculate a mass flux of 3087 $\text{kg/m}^2\text{/s}$, an inlet density of 15.38 kg/m^3 and a flow density of 9.728 kg/m^3. Solution of the static force balance yields a K_b value of 0.05 (see Figure 16) which is consistent with industry experience of when the valve will start to lift initially at around 5 % overpressure.

The force balance governing the disk motion is a fundamental balance. The net force balance indicates that the behavior of the valve will be different for different fluid types and molecular weights. Different fluids will yield different mass flux and density values. A valve specific K_b curve developed with air as a fluid will not directly apply to hydrogen for example. The fundamental force balance with parameters developed from the air specific K_b curve will be more appropriate and is recommended.

Figure 14: Consolidated reported K_b curve for 1900 series balanced bellows valve, vapors and gases

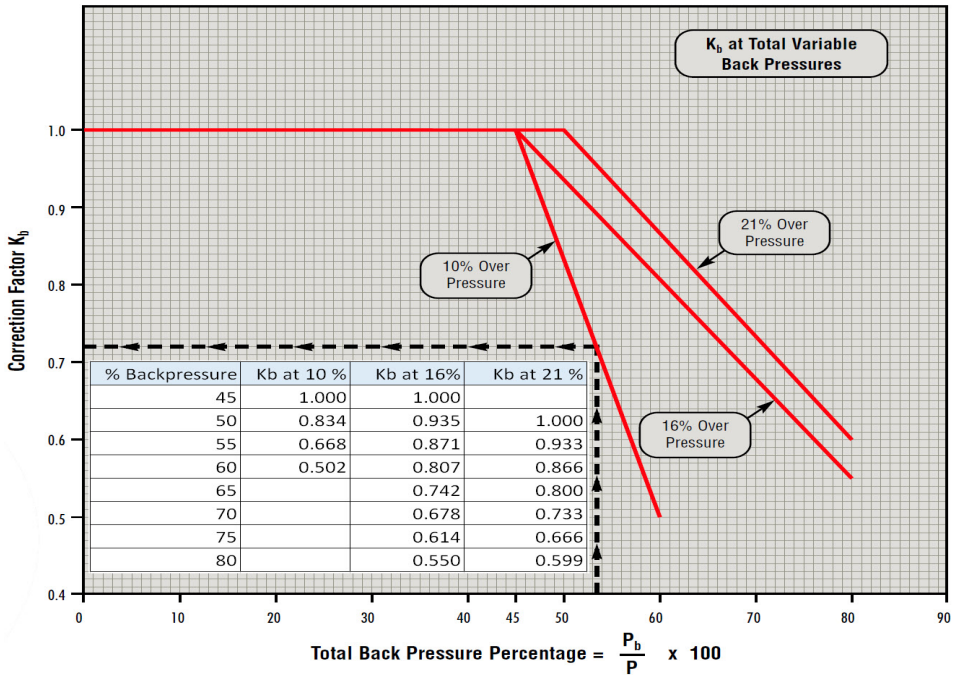

% Backpressure	Kb at 10 %	Kb at 16%	Kb at 21 %
45	1.000	1.000	
50	0.834	0.935	1.000
55	0.668	0.871	0.933
60	0.502	0.807	0.866
65		0.742	0.800
70		0.678	0.733
75		0.614	0.666
80		0.550	0.599

Figure 15: Static force balance predictions of K_b using best regression values of $\theta_o = 74.56$ degrees, $\psi = 0$, and $\eta = 0.591$

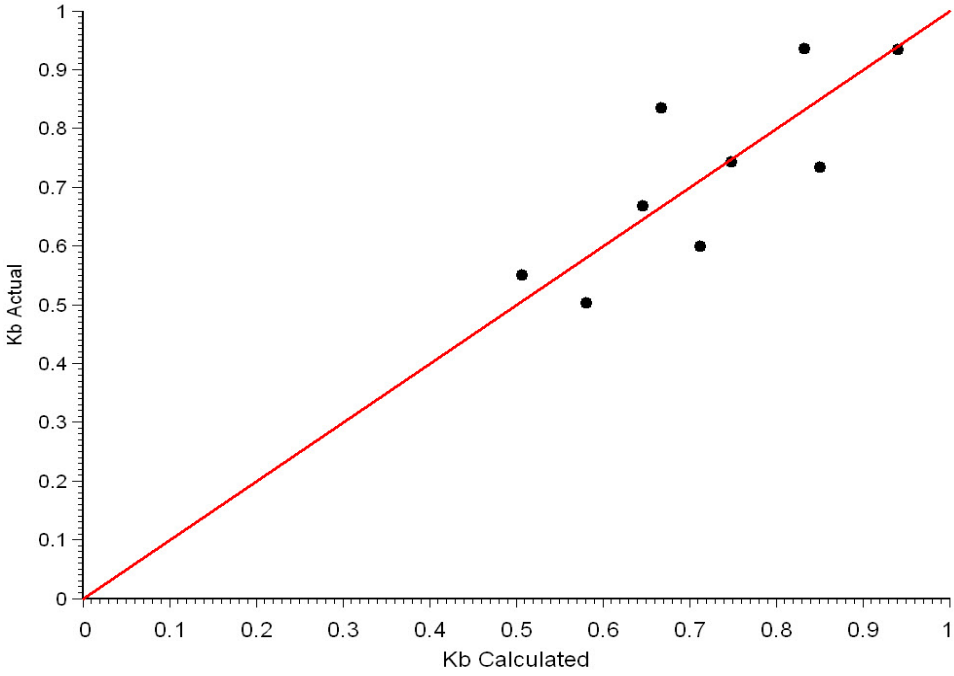

Table 2: Data required for force balance parameter regression for vapor service

Variable	Point 1	Point 2	Point 3
Overpressure	10 %	10 %	10 %
P_N, Pa	1504409	1504409	1504409
ρ_N, $\mathrm{kg/m^3}$	17.643	17.643	17.643
P_B, Pa	739090	802866	866643
G, $\mathrm{kg/m^2/s}$	3540.70	3540.20	3521.00
ρ_e, $\mathrm{kg/m^3}$	11.181	11.321	11.951
K_b	0.834	0.668	0.502
Overpressure	16 %	16 %	16 %
P_N, Pa	1580940	1580940	1580940
ρ_N, $\mathrm{kg/m^3}$	18.547	18.547	18.547
P_B, Pa	739090	930419	1121749
G, $\mathrm{kg/m^2/s}$	3722.16	3690.27	3434.40
ρ_e, $\mathrm{kg/m^3}$	11.75	12.758	14.561
K_b	0.935	0.742	0.55
Overpressure	21 %	21 %	21 %
P_N, Pa	1644716	1644716	1644716
ρ_N, $\mathrm{kg/m^3}$	19.301	19.301	19.301
P_B, Pa	739090	994196	1121749
G, $\mathrm{kg/m^2/s}$	3873.49	3820.85	3659.71
ρ_e, $\mathrm{kg/m^3}$	12.236	13.532	14.737
K_b	0.933	0.733	0.599

Figure 16: Static force balance predictions of K_b using best regression values of $\theta_o = 74.56$ degrees, $\psi = 0$, and $\eta = 0.591$ for $P_N = 175.75$ psig and $P_b = 64.75$ psig

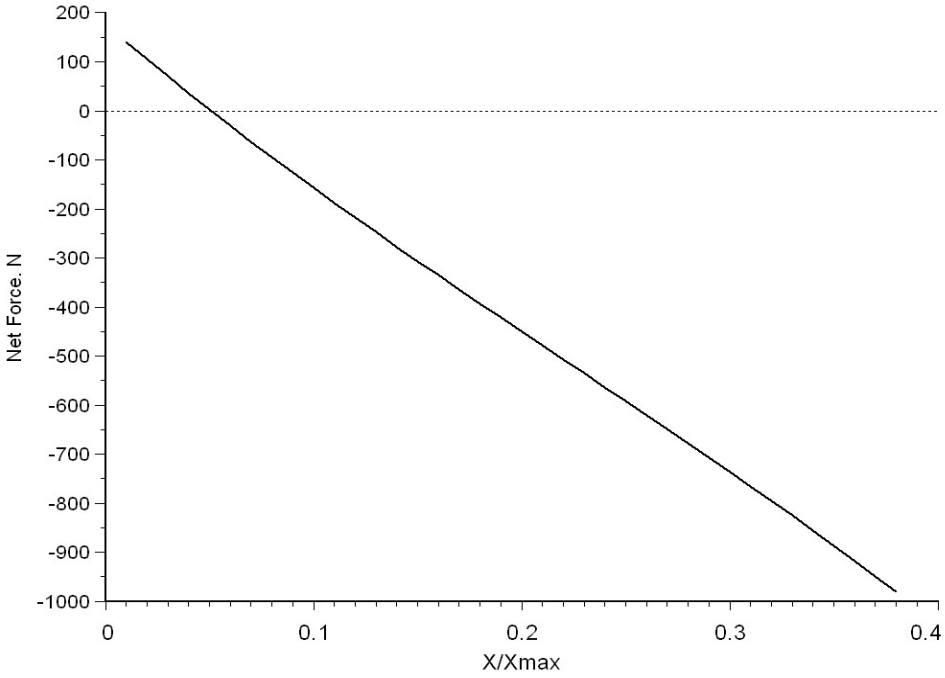

The same parameter estimation can also be conducted for the same balanced bellows valve in liquid service for water. In this case the liquid mass flux can be calculated analytically using Bernoulli's equation and the nozzle inlet and flow densities are constant for water. Consolidated reports the a K_w curve for the 1900 series as shown in Figure 17. We select three points from the K_w curve as shown in Table 3. The regressed parameters are shown in Figure 18. Once again the best estimated value of ψ is 0, indicating that the discharge coefficient value to be is a constant. In this particular case the value reported by Consolidated is 0.669 for a flow area of 12.85 in^2 or 0.69 for a flow area of 12.47 in^2.

The static force balance best fit of parameters for liquid and gas service yielded on best value of $\psi = 0$. This finding is confirmed by the PERF-I data set. The effective discharge coefficient of the

Table 3: Data required for force balance parameter regression for liquid service

Variable	Point 1	Point 2	Point 3
Overpressure	10 %	10 %	10 %
P_N, Pa	1504409	1504409	1504409
ρ_N, kg/m^3	1000	1000	1000
P_B, Pa	611537	866643	1108994
G, $\text{kg/m}^2/\text{s}$	$\sqrt{2\rho\left(P_N - P_B\right)}$	$\sqrt{2\rho\left(P_N - P_B\right)}$	$\sqrt{2\rho\left(P_N - P_B\right)}$
ρ_e, kg/m^3	1000	1000	1000
K_b	0.8	0.5	0.2

Figure 17: Consolidated reported K_w curve for 1900 series balanced bellows valve in liquid service

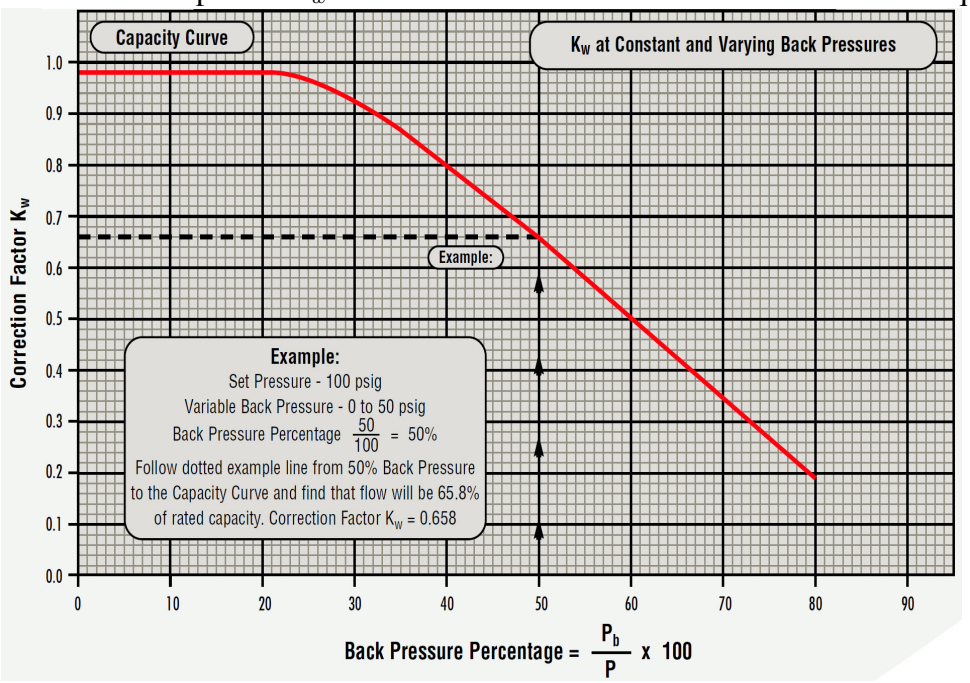

Figure 18: Static force balance predictions of K_w using best regression values of $\theta_o = 90$ degrees, $\psi = 0$, and $\eta = 0.525$

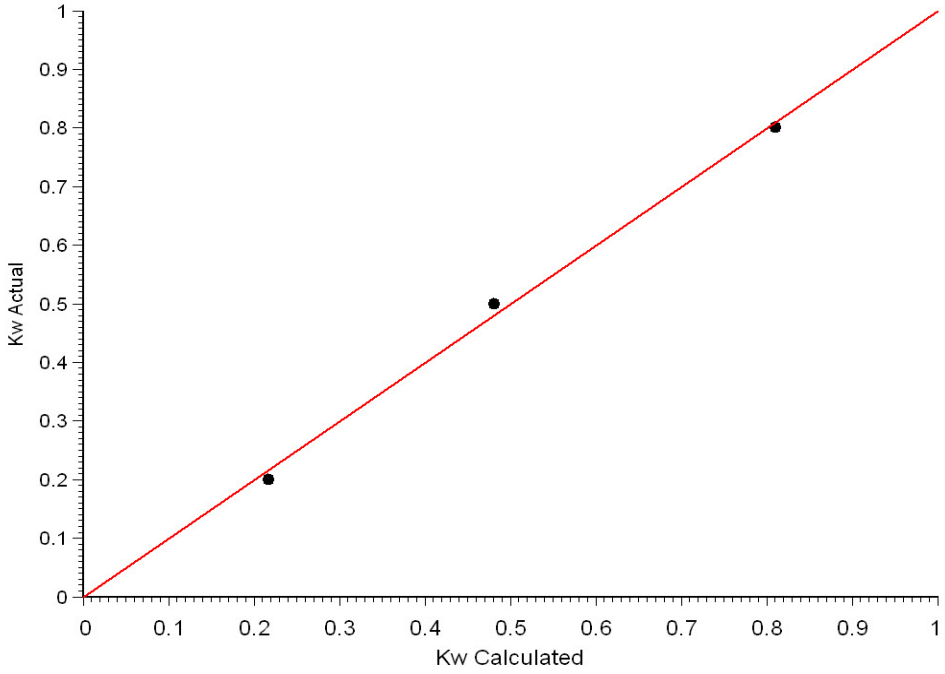

Figure 19: 2J3 air flow vs. overpressure, $P_{set} = 250$ psig [1]

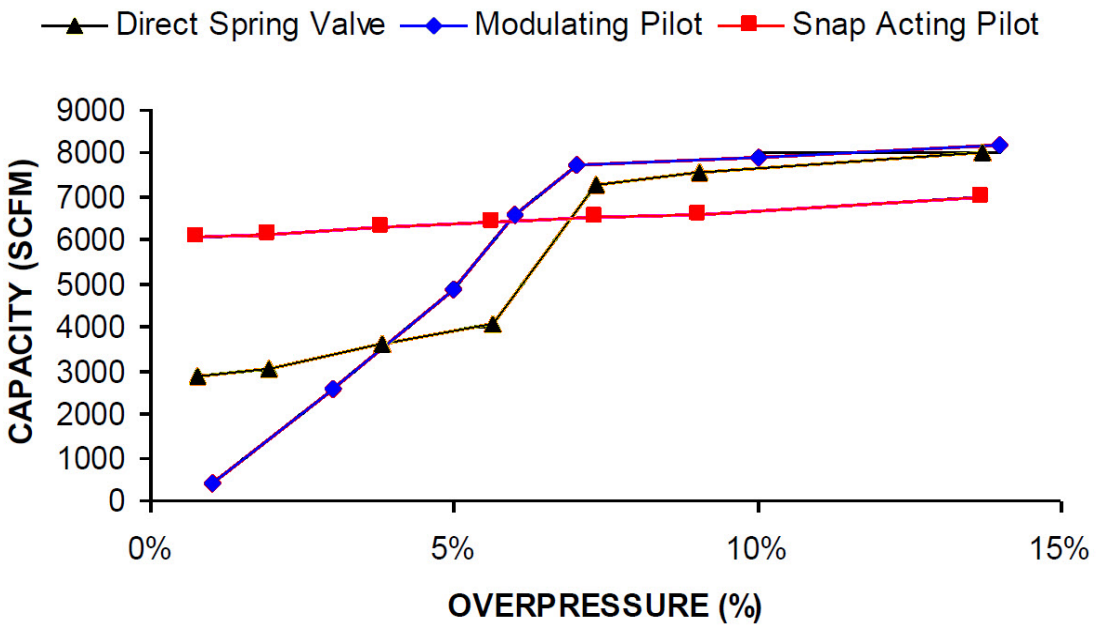

valves was measured at 5 % increments of disk lift and was found to agree closely with the fully open discharge coefficient value when based on the actual flow area.

18.3 PRV Flow vs. Overpressure Data

PRV SDOF parameters can also be regressed where PRV flow capacity vs. overpressure data is available from the manufacturer or from actual testing. For example, Buxton [1] provided flow capacity data for an API 526 conventional spring loaded valve. The data was reported for a 2J3 set at 250 psig with an actual flow area of 1.453 in^2 and a discharge coefficient at maximum lift of 0.967 (estimated from actual flow data at 15 % overpressure for air flow). An isentropic flow calculation for air yields a flow capacity of 7750 SCFM of air at 15 % overpressure and full lift as shown in Figure 19. At an overpressure less than 10 %, such as 5 %, the PRV is flowing at reduced but stable lift. The actual flow area is limited by the curtain flow area, $A_c = 2\pi R_N x$ and the effective flow area will be given by $C_d A_c$ where $C_d = \psi C_{d,max} = 0.967\psi$. Using three points from the linear portions of the flow capacity vs. % overpressure, we can estimate the values of η, θ_o, and α that best reproduce the reduced lift (flow capacity) at those points. This data confirms that an assumption of $\psi = 0.9$ provides a very good estimate of ψ.

Similar data was provided by Buxton [1] for liquid water flow as shown in Figure 20.

Figure 20: 2J3 water flow vs. overpressure, $P_{set} = 250$ psig [1]

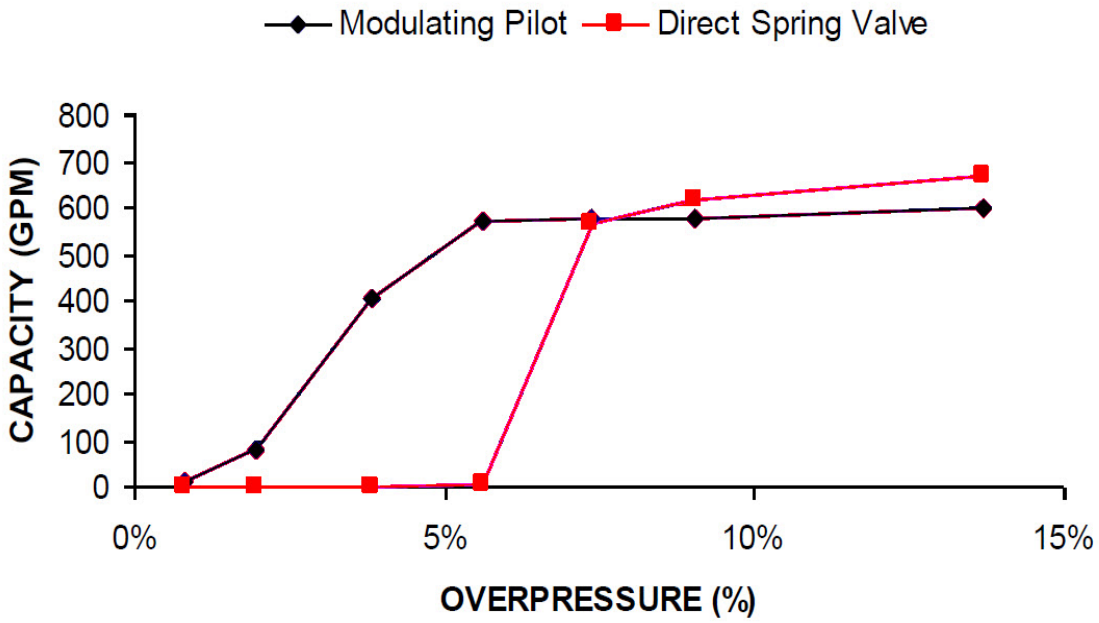

19 PRV Stability in Liquid Service

The water hammer solutions described earlier can be extended to PRVs in liquid service. The water hammer right flow boundary condition depended on a the timed closure of the valve. We can easily modify this right boundary condition such that valve closure and opening will depend on the pressure at the disk surface of the PRV. The dynamics of the valve opening and closing are solved simultaneously with the fluid flow dynamics equations.

To illustrate the importance of the pressure wave interaction with the valve disk during valve closure and opening, we use the same 6Q8 Consolidated valve considered in earlier examples. The left boundary stagnation pressure of the inlet line is set at 10 % over the set pressure (185 psig). We then vary the inlet line length but keep the diameter constant at 6 inches. Note that the right boundary flow area must correspond to the nozzle flow are of the PRV. The flow area of the inlet pipe is reduced to the nozzle flow area at the right boundary. We assume in this case a constant atmospheric backpressure without a discharge pipe so that we can only study the interaction effect between line length and PRV disk motion.

PRV stability issues are amplified in liquid service. The speed of sound in liquid service is large (1220 ms/ for this example). As soon as the valve starts to open, the pressure at the disk will start to drop very rapidly as flow is established. The returning pressure wave can keep the valve open but also can cause chatter or flutter if the pressure wave frequency in the inlet line couples with the valve opening and closing frequency. The dynamic reaction forces can also be very large in liquid systems due to the water hammer type pressures encountered when the valve closes suddenly during chatter or flutter. If the inlet line is much longer that the critical chatter line length, the PRV can operate in a stable manner. This will be shown in our simulations and has been demonstrated

experimentally by Izuchi [2, 3].

We considered inlet line lengths of 0.1, 1, 2, 5, 7, 10, 15, 25, and 50 meters. A fixed grid size of 0.01 m was used. We note from Figure 21 that the PRV operates in a stable manner for inlet lines lengths up to 2 meters. Instability (flutter) starts at 5 meters although the 5 meters case results in stable behavior. The cases involving 7 and 10 meters are unstable with valve chatter. Increasing the inlet line lengths to 15 meters results in quasi-stable (flutter) behavior again. Note that although stable behavior is regained, the flow capacity of the valve is reduced as shown by the maximum valve lift reached. The calculated valve opening time is approximately 45 milliseconds which is very close to the opening time calculated with an inlet line length of 0.1 m.

It is very clear from these estimates that PRV instability (chatter and flutter) results from the coupling of the pressure wave in the inlet line and the PRV disk motion. There is no resonance because the PRV disk instability is not amplified but merely persists for as long as the source pressure remains at the same level.

The 50 meters case is worthy of a special discussion. The PRV initially reaches multiple instances of stable behaviors that last approximately 50 milliseconds each. The PRV lift jumps from one static position to a higher one after 50 milliseconds. These jumps become smaller and ultimately disappear as the valve reaches a steady state lift. This behavior may have been identified by Pentair [4] in a recent presentation to API. The jumps from one quasi-steady state to another become more pronounced at 100 meters.

Figure 22 illustrates the dynamic reaction forces exhibited upstream of the valve for the 10 meter solution. These solutions are also animated and are provided as Windows .AVI files so that one can see the progression of instability. Note the reaction forces are in kilo Newtons and are extremely large and last long enough to cause damage to most piping systems. This type of behavior is consistent with industry experience showing that more damage is observed with PRV chatter in liquid service.

The same solution is also demonstrated for all vapor service using methane as fluid. Similar behavior is shown except that the dynamic reaction forces are much smaller.

20 Modeling PRV Stability Data Needs

In order to properly model the behavior of a spring load pressure relief valve, we need the following information:

1. Accurate valve geometry information for A_D, A_N, A_{bel}, and A_I,
2. valve body volume,
3. mass of the spring and moving parts m_D,
4. ψ and η parameters,
5. critical damping ratio, ζ,

Figure 21: Impact of inlet line length on PRV stability in liquid service

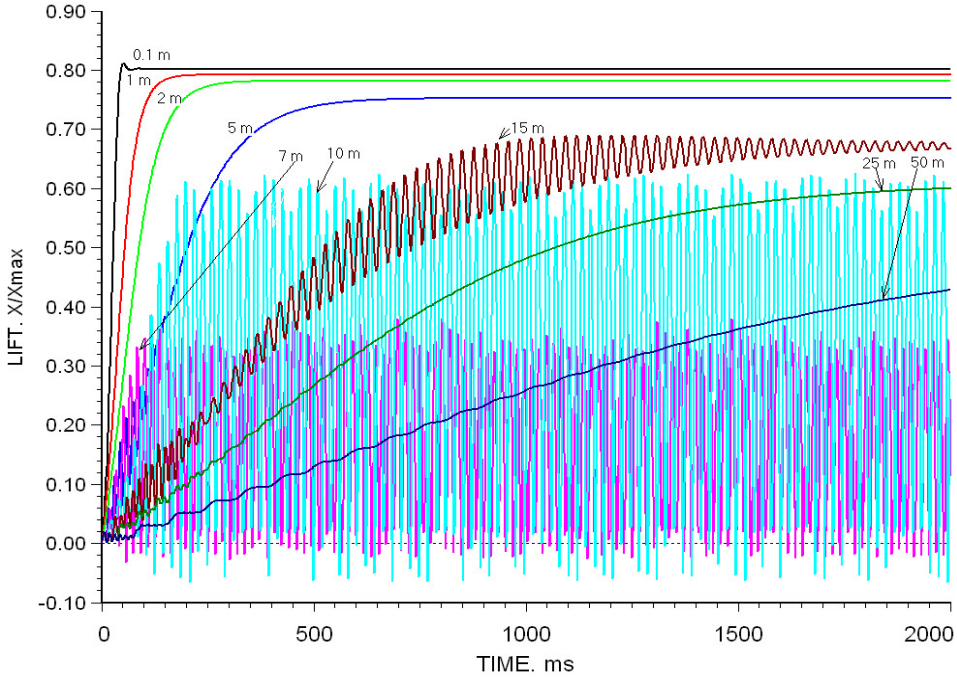

Figure 22: Dynamic reaction force loads at vessel connection (x=0) upstream of the 6Q8

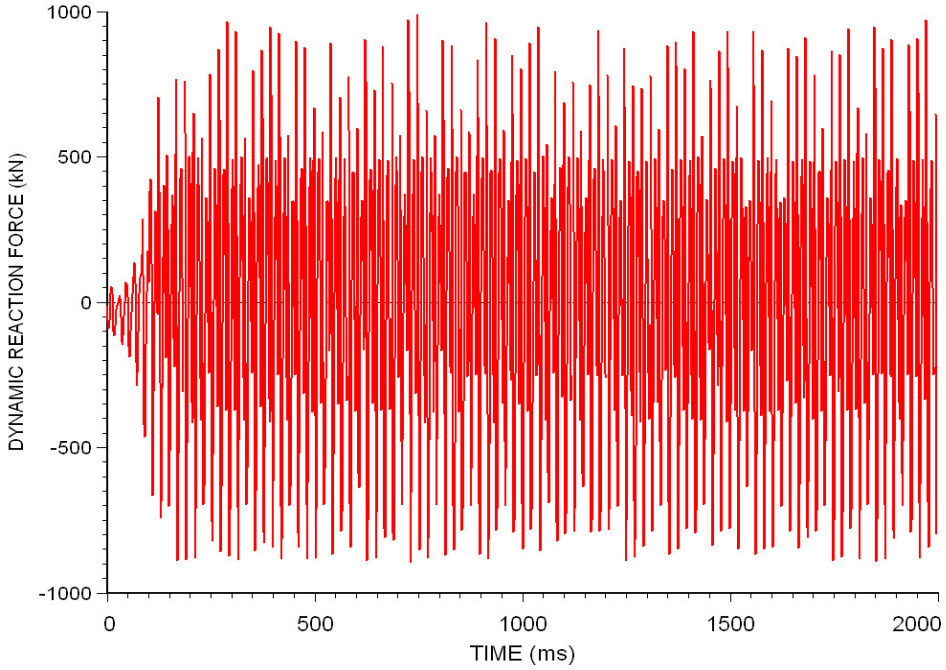

6. fluid exit discharge angle at full lift θ_o, and

7. spring constant K_s and bellows stiffness constant K_{sb}.

Although Izuchi [2, 3] and Pentair [4, 5, 6, 7, 8] established experimental curve for valve lift vs. pressure to use in their modeling efforts, many of the parameters listed above can be established from already published data. The availability of actual test data can improve the predictive capabilities of the models established in this paper.

21 SuperChems Expert Solution

The SuperChems PRV stability model integrates four key components:

Dynamic Vessel Model This is a detailed dynamic model that already exists in SuperChems for reacting single and multiphase systems.

Inlet Piping Model This is an existing detailed piping flow model for single and multiphase reacting flow. This model is coupled with the dynamic vessel model to provide the inlet pressure loss and fluid conditions at the inlet of the PRV.

Discharge Piping Model This is an existing detailed piping flow model for single and multiphase reacting flow. This model is coupled with the dynamic vessel model to provide the back pressure and fluid conditions at the discharge of the PRV. This model performs the shock discontinuity calculations.

Dynamic PRV Model This is detailed dynamic model based on a modification of the method developed by Singh and Shak [9]. This model relies on the existing detailed SuperChems dynamic vessel and piping models to calculate the fluid conditions at the inlet and discharge of the PRV for a specified user time step.

Equations 39, 47, 61, 65, 12, 17, 20, 26, 27, 35, and 36 can be integrated numerically over a specified time step with user specified values of P_I, P_B, ρ_I, and $\dot{m}$. The SuperChems solution is performed using time splitting:

Step 1: Set $t = 0$, $u_d = 0$ and $x = 0$. Set P_B to ambient pressure or user superimposed back pressure. Set P_I and ρ_I to vessel conditions P_o and ρ_o. Set $\dot{m}$ to 0.

Step 2: Assume that P_B, ρ_I, and $\dot{m}$ persist for one time step, dt

Step 3: Integrate Equations 12, 17, 20, 26, 27, 35 and 36 for one time step dt.

Step 4: Set the PRV flow area to the smaller value of either A_N or $2\pi R_1 x$. Set the discharge coefficient for the PRV from Equations 26 and 27.

Step 5: Solve the coupled vessel-piping dynamics using the existing detailed and complex SuperChems Models for one time step dt.

Step 6: Set P_I and ρ_I to the values calculated at the inlet of the PRV. Set the value of P_B to the value calculate at the discharge of the PRV. Set $\dot{m}$ to the value calculated by the vessel dynamics.

Step 7: Increment time by dt.

Step 8: Go to Step 2.

22 Conclusions

We developed in this paper a detailed dynamics model for the modeling of PRV stability in relief systems. Through this detailed modeling we established that (a) the irrecoverable inlet pressure loss due to friction has essentially no impact on PRV stability (also see [4]), (b) PRV instability is caused by the coupling of PRV disk motion with the pressure wave caused by excessive dynamic pressure drop (1/4 wave) during PRV opening, (c) the instability does not amplify, and (d) liquid systems are the most likely to cause damage to piping and piping components.

References

[1] C. Buxton. Modulating PRV performance data. In *API 520 Committee Meeting Minutes*. Amperican Petroleum Institute, 2003.

[2] Hisao Izuchi. Stability analysis of safety valve. In *10th Topical Conference on Gas Utilization*. AIChE, AIChE, 2010.

[3] Hisao Izuchi. Chatter of safety valve. In *Presentation to API 520 Committee*. API, API, 2008.

[4] Kenneth Paul, Michael McNeely, Csaba Hos, and Alan Champneys. Dynamics of gas direct spring-loaded pressure relief valves. In *API 78th Fall Refining and Equipment Standards Meeting*. API, 2013.

[5] C. J. Hos, A. R. Champneys, K. Paul, and M. McNeely. Dynamic behavior of direct spring loaded pressure relief valves in gas service: II reduced order modelling. *Journal of Loss Prevention in the Process Industries*, 36:1–12, 2015.

[6] C. J. Hos, A. R. Champneys, K. Paul, and M. McNeely. Dynamic behavior of direct spring loaded pressure relief valves: III valves in liquid service. *Journal of Loss Prevention in the Process Industries*, 43:1–9, 2016.

[7] C. J. Hos, A. R. Champneys, K. Paul, and M. McNeely. Dynamic behavior of direct spring loaded pressure relief valves connected to inlet piping: IV review and recommendations. *Journal of Loss Prevention in the Process Industries*, 48:270–288, 2017.

[8] K. Paul. Dynamic behavior of direct spring loaded pressure relief valves - a review of stability concerns. In *Spring DIERS Users Group Meeting, Houston, Texas*. DIERS, AIChE, 2016.

[9] A. Singh and D. Shak. Modeling of a spring loaded safety valve. In *Testing and Analysis of Safety / Relief Valve Performance*, pages 63–70. American Society of Mechanical Engineers, ASME, 1983.

[10] A. Singh. An analytical study of the dynamics and stability of a spring loaded safety valve. *Nuclear Engineering and Design*, 72:197–204, 1982.

[11] A. Singh, A. M. Hecht, and M. E. Teske. A model for predicting the performance of spring loaded safety valves. In *Testing and Analysis of Safety / Relief Valve Performance*, pages 47–54. American Society of Mechanical Engineers, ASME, 1983.

[12] Frederick J. Moody. *Introduction to Unsteady Thermofluid Mechanics*. Wiley, 1990.

[13] G. A. Melhem. Analysis of PRV stability in relief systems. Part IX - body bowl choking and multiple chokes. *ioMosaic Corporation Publication*, October 2024.

[14] G. A. Melhem. Understanding PRV stability - body bowl choking. In *PRV Stability Workshop, Houston*. ioMosaic, September 2019.

[15] H. Izuchi. Effect of body bowl choking on pressure relief valve stability. In *11th Global Congress on Process Safety*. AIChE, April 2015.

[16] G. A. Melhem. Analysis of PRV stability in relief systems. Part IV - On the estimation of speed of sound and thermodynamic properties for fluid flow and prv stability. *ioMosaic Corporation Publication*, 2017.

[17] A. Beune, J. G. M. Kuerten, and J. Schmidt. Numerical calculation and experimental validation of safety valve flows at pressure up to 600 bar. *AIChE Journal*, 57, December 2011.

[18] J. E. Huff. Intrinsic back pressure in safety valves. *API Refining Meeting Proceedings*, 62:105–111, 1983.

[19] G. A. Melhem and G. Hendrickson. Quantify non-equilibrium flow and rapid phase transitions (RPT). *ioMosaic Corporation Publication*, 2020.

[20] G. Hendrickson, G. A. Melhem, R. D'Alessandro, H. Fisher, M. Levin, D. Smith, and L. Korelstein. Geometric and thermodynamic considerations of saturated and slightly subcooled water flow through nozzles. *Chemical Engineering Science*, 254:1–16, 2022.

[21] J. C. Leung. Easily size relief devices and piping for two-phase flow. *Chemical Engineering Progress*, 92(12):28–49, 1996.

[22] J. Leung. Sizing of pressure relief devices and associated piping for multiphase flows. In *2nd International Symposium on Runaway reactions, Pressure Relief Design and Effluent Handling, G. A. Melhem and H. G. Fisher, Editors*, pages 319–351. DIERS, AIChE, 1998.

[23] J. Leung. A non-equilibrium flow model for initially saturated and subcooled liquid discharge. In *DIERS EDUG Meeting, Hamburg, Germany*. EDUG, June 2011.

[24] G. A. Melhem. A general purpose method for the estimation of multiple chokes in gas-vapor and two-phase flow. In *DIERS Users Group Meeting*. AIChE, October 1997.

[25] N. A. Joukowsky. A translation of joukowsky's paper on water hammer experiments. *Journal of the American Waterworks Association*, page 335, 1904.

[26] T. W. Walters and R. A. Leishear. When the Joukowsky equation does not predict maximum water hammer pressure. *Journal of Pressure Vessel Technology*, 141:060801–1:10, December 2019.

[27] B. Jung, P. Boulos, D. Wood, and C. Bros. A Lagrangian wave characteristic method for simulating transient water column separation. *Journal of the American Water Works Association AWWA*, 101:6:64–73, 2009.

[28] G. A. Melhem. Analysis of PRV stability in relief systems. Part II - Screening. *ioMosaic Corporation Publication*, 2014.

[29] Y. S. Lai. Performance of a safety relief valve under back pressure conditions. *Journal of Loss Prevention in the Process Industries*, 5(1):55–59, 1992.

[30] M. A. Grolmes. Odds and ends - relief valve stability - Part 4. In *DIERS Users Group Meeting*. American Society of Chemical Engineers, AIChE/DIERS, 2011.

....

Index

About the Authors

Dr. Melhem is an internationally known pressure relief and flare systems, chemical reaction systems, process safety, and risk analysis expert. In this regard he has provided consulting, design services, expert testimony, incident investigation, and incident reconstruction for a large number of clients. Since 1988, he has conducted and participated in numerous studies focused on the risks associated with process industries fixed facilities, facility siting, business interruption, and transportation.

Prior to founding ioMosaic® Corporation, Dr. Melhem was president of Pyxsys Corporation; a technology subsidiary of Arthur D. Little Inc. Prior to Pyxsys and during his twelve years tenure at Arthur D. Little, Dr. Melhem was a vice president of Arthur D. Little and managing director of its Global Safety and Risk Management Practice and Process Safety and Reaction Engineering Laboratories.

Dr. Melhem holds a Ph.D. and an M.S. in Chemical Engineering, as well as a B.S. in Chemical Engineering with a minor in Industrial Engineering, all from Northeastern University. In addition, he has completed executive training in the areas of Finance and Strategic Sales Management at the Harvard Business School. Dr. Melhem is a Fellow of the American Institute of Chemical Engineers (AIChE) and Vice Chair of the AIChE Design Institute for Emergency Relief Systems (DiERS).

Contact Information

Georges. A. Melhem, Ph.D., FAIChE
E-mail. melhem@iomosaic.com

ioMosaic Corporation
93 Stiles Road
Salem, New Hampshire 03079
Tel. 603.893.7009, x 1001
Fax. 603.251.8384
web. www.iomosaic.com

How can we help?

Please visit www.iomosaic.com and www.iokinetic.com to preview numerous publications on process safety management, chemical reactivity and dust hazards characterization, safety moments, video papers, software solutions, and online training.

In addition to our deep experience in process safety management (PSM), chemical reaction systems, and the conduct of large-scale site wide relief systems evaluations by both static and dynamic methods, we understand the many non-technical and subtle aspects of regulatory compliance and legal requirements. When you work with ioMosaic® you have a trusted ISO certified partner that you can rely on for assistance and support with the lifecycle costs of relief systems to achieve optimal risk reduction and PSM compliance that you can evergreen. We invite you to connect the dots with ioMosaic®.

We also offer laboratory testing services through ioKinetic® for the characterization of chemical reactivity and dust/flammability hazards. ioKinetic® is an ISO accredited, ultramodern testing facility that can assist in minimizing operational risks. Our experienced professionals will help you define what you need, conduct the testing, interpret the data, and conduct detailed analysis. All with the goal of helping you identify your hazards, define and control your risk.

ioMosaic®
Minimizing risk. Maximizing potential.®

About ioMosaic Corporation

Our mission is to help you protect your people, plant, stakeholder value, and our planet.

Through innovation and dedication to continual improvement, ioMosaic has become a leading provider of integrated process safety and risk management solutions. ioMosaic has expertise in a wide variety of disciplines, including pressure relief systems design, process safety management, expert litigation support, laboratory services, training, and software development.

As a certified ISO 9001:2015 Quality Management System (QMS) company, ioMosaic offers integrated process safety and risk management services to help you manage and reduce episodic risk. Because when safety, efficiency, and compliance are improved, you can sleep better at night. Our extensive expertise allows us the flexibility, resources, and capabilities to determine what you need to reduce and manage episodic risk, maintain compliance, and prevent injuries and catastrophic incidents.

Consulting Services

- Asset Integrity
- Auditing
- Due Diligence
- Facility Siting
- Fault Tree/SIL Analysis
- Fire & Explosion Dynamics
- Incident Investigation, Litigation Support, and Expert Testimony
- Hydrogen Safety
- LNG Safety
- LPG Safety
- Pipeline Safety
- Process Hazard Analysis
- Process Engineering Design and Support
- Process Safety Management
- Relief and Flare Systems Design and Evaluation
- Risk Management Program Development
- Quantitative Risk Assessment
- Software Solutions
- Structural Dynamics
- Sustainability Reporting Support
- Technology Transfer Package Development
- Process Safety Training

Laboratory Testing Services (ISO Accredited)

- Battery Safety Testing
- Chemical Reactivity Testing
- Combustible Dust Hazard Analysis and Testing
- Flammability Testing
- Physical Properties Testing
- Process Safety Services
- Specialized Testing

US Offices

Salem, New Hampshire
Houston, Texas
Minneapolis, Minnesota
Berkeley, California

International Offices

Al Seef, Kingdom of Bahrain
Bath, United Kingdom

Software Solutions

Process Safety Office®: A suite of integrated tools for process safety professionals and risk analysts.

Process Safety Enterprise®: Process Safety Management compliance made easy with enterprise workflows, dynamic forms, document management, key performance indicators and metrics, and more.

Process Safety Learning®: Build your process safety competencies incrementally using learning modules.

Process Safety tv®: The worldś first video streaming platform dedicated to process safety.

Contact us

www.ioMosaic.com
sales@ioMosaic.com
1.844.ioMosaic